STRUCTURAL CONTROLS ON THE EDWARDS AQUIFER/TRINITY AQUIFER INTERFACE IN THE HELOTES QUADRANGLE, TEXAS

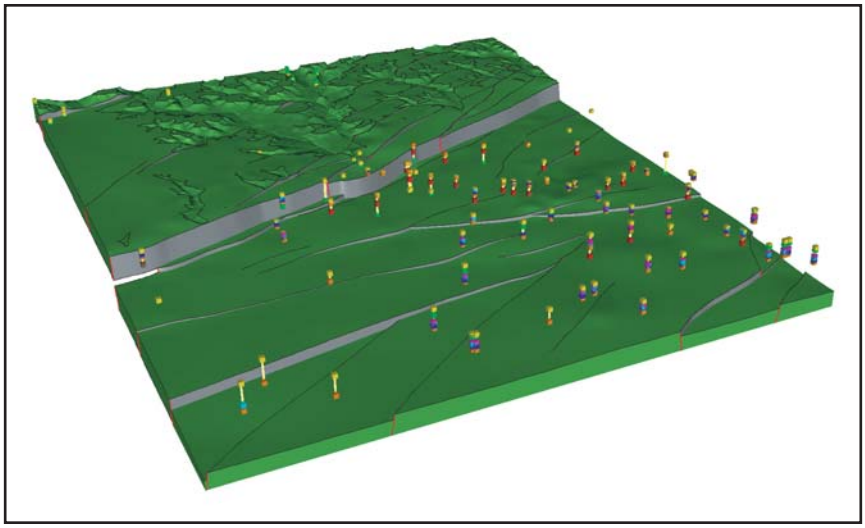

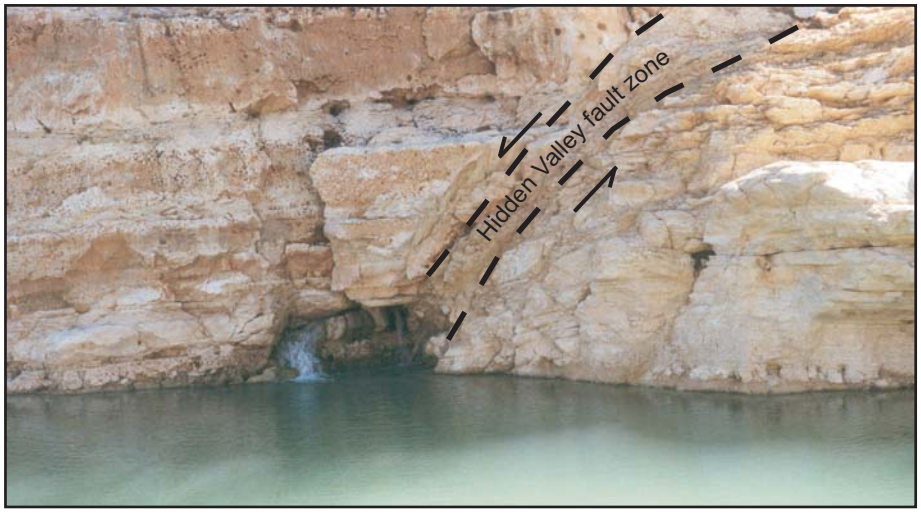

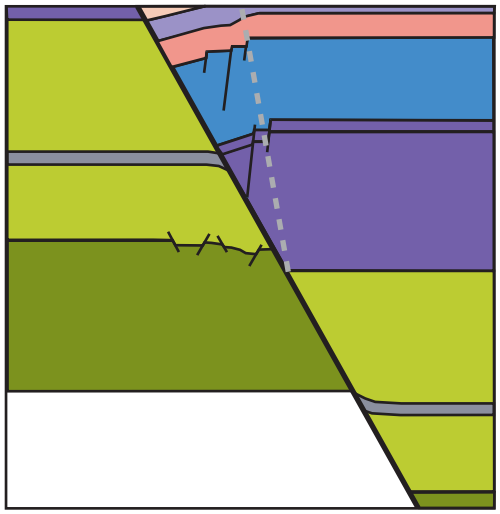

REVISED
FEBRUARY 2005

Structural Controls on the Edwards Aquifer/Trinity Aquifer Interface in the Helotes Quadrangle, Texas

David A. Ferrill[1], Darrell W. Sims[1], Nathan Franklin[1], Alan P. Morris[2], Deborah J. Waiting[1]

[1] CNWRA, Southwest Research Institute®, San Antonio, TX 78238-5166

[2] Department of Earth and Environmental Science, University of Texas at San Antonio, San Antonio, TX 78249

Prepared for:

Edwards Aquifer Authority and

U.S. Army Corps of Engineers

December 24, 2004

Revised February 4, 2005

EXECUTIVE SUMMARY

The purpose of the project reported here is to characterize the structural architecture of the Edwards and Trinity Aquifers in the area of the Helotes 7 ½ minute quadrangle. Included in this analysis are tasks to generate a three-dimensional computer model (geologic framework model) of the Edwards and Trinity Aquifers, and perform field investigations to characterize the mechanisms and products of localized fault-related deformation in the Edwards and Trinity Aquifers in and near the study area. An important objective is to analyze the potential for groundwater flow from the Trinity Aquifer to the Edwards Aquifer, taking into account fault-related deformation and juxtaposition of the aquifers across key faults.

Results of the project show the aquifer architecture throughout the study area, the location and interpreted geometry of the most important mapped faults in the study area, and the deformation mechanisms and deformation style in fault zones in the rocks of both the Edwards and Trinity Aquifers. The three-dimensional geologic framework model of the Helotes area reveals: (i) juxtaposition of permeable and relatively impermeable hydrogeologic units, (ii) structural thinning of the Edwards and Trinity Aquifers, (iii) potential for cross-fault communication between the Edwards and Trinity Aquifers, (iv) faults expressed on the surface as potential infiltration pathways, and (v) maximum offset concentrated along a small number (two or three) faults. This information, along with an understanding of fault zone deformation mechanisms and the role of fault zones as barriers or conduits, can assist in locating environmentally sensitive areas. It is useful for aquifer water flow path studies and contributes to the identification of areas where communication between the Trinity and Edwards Aquifers is suspected.

In this geologic framework model, the Edwards and Trinity Aquifers and associated confining layers are subdivided into 12 stratigraphic units which are offset by a network of 30 faults. Vertical offset (fault throw) ranges from near zero to an approximate maximum of 178 meters (584 ft). Displacement sense is normal, commonly down to the southeast, and lateral throw gradients are generally small (0.002 to 0.015), although locally may be as high as 0.03. In map view, fault blocks are elongate, with the long axis commonly oriented NE-SW. Maximum offset is concentrated along two major fault systems; one fault, the Haby Crossing fault, has a maximum throw of about 178 m (584 ft) and juxtaposes virtually the entire Edwards Group stratigraphic section with rocks of the Glen Rose Formation beneath the City of Helotes. The Diversion Lake fault cuts across the NW corner of the Helotes Quadrangle, and has a maximum throw of 68 m (223 ft) within the quadrangle area.

In general, normal faults of all displacements decrease the effective aquifer thickness. This structural thinning of aquifer layers can cause flow constrictions, which in turn may divert flow and cause fluctuations in the local water table from fault block to fault block. Areas of such flow constrictions can be identified using a map of fault throw distribution; constriction is likely greatest where fault throw is greatest.

The large displacement on the Haby Crossing fault within the Helotes quadrangle may be significant for direct communication between the Edwards Group and Glen Rose Formation in this area. Also important, this large displacement on a single fault is responsible for dropping the Edwards Aquifer from hilltop exposures north of the Haby Crossing fault, to mostly buried (confined) on the south side. Consequently, this large-displacement fault results in a local narrowing of the area designated as Edwards Aquifer recharge zone.

3DStress™ analyses of measured faults and regional stratigraphic thicknesses based on published maps yield a stress system during faulting of: vertical effective stress = 15 MPa; minimum horizontal effective

stress (σ_3') = 4 MPa with an azimuth of 150°; and an intermediate principal effective stress = 9.5 MPa. When applied to the fault surfaces exported from the three-dimensional geologic framework model, this stress tensor indicates that the dominant, NE-SW striking faults experience high slip tendencies and are well oriented to have accommodated regional strains developed within the inferred stress system. In addition to experiencing high slip tendencies in the inferred stress system, the predominant faults are also subject to high dilation tendencies; this is especially true within the Edwards Aquifer section because these faults tend to have steeper dips than those within the Glen Rose Formation, and hence experience greater dilation tendencies. This combination of high slip and dilation tendencies implies that the major faults could have been effective fluid transmission pathways at the time of faulting. If a similar stress system were extant today, the faults would be in favorable orientations for enhanced fluid transmissivity.

Fault block deformation calculated using cutoff lines generated from the three-dimensional geologic framework model results in cutoff line elongations that rarely exceed 2 percent (positive or negative). Although these small cutoff elongations reflect generally low displacement gradients, faults within the Helotes area exhibit higher cutoff strains along more fault length than either the Castle Hills or Camp Bullis areas. At the scale of the three-dimensional model, competent units exhibit gentle dips, which is consistent with relatively rapid lateral and vertical fault propagation, until intersection with other faults occurs (laterally) or intersection with a weaker mechanical layer occurs. The overall lack of steep lateral displacement gradients suggests rapid fault propagation with respect to the rate of displacement accumulation on the faults, although there are locations in which steeper lateral gradients have developed.

Field work reveals interesting contrasts between faults in the Edwards and Trinity Aquifers. Faults with displacements of 5 m (16 ft) to tens of meters in the Glen Rose Formation (Trinity Aquifer) commonly have wide damage zones, on the order of meters, within which small faults, rotated fault blocks, and smear of clay shale beds (if present) are common. By contrast fault zones with displacements of 5 m (16 ft) to tens of meters in the Edwards Group limestones typically have numerous associated small faults, but associated block rotation and bed tilting are rare. This characteristic difference in structural style between the Edwards Group limestones and the Glen Rose Formation appears to be related to lithologic differences and the resulting differences in mechanical behavior of the two stratigraphic sections. The Glen Rose Formation contains both competent massive limestone beds and incompetent argillaceous limestone and shale beds. Incompetent beds tend to arrest fault propagation during fault growth. Consequently, with increasing fault displacement, fault tips (terminations) episodically propagate. Continued displacement on a fault with an arrested fault tipline will produce fault tipline folding and associated local deformation such as complex small-scale faulting. Resulting fault damage zones are quite complex and variable along a fault, and the complexity of faulting is related to the structural position (including displacement magnitude) and the associated mechanical stratigraphy. Permeability in fault zones and fault blocks is strongly influenced by deformation styles in different mechanical layers as well as the deformation progression with increasing fault displacement.

The large fault surfaces that cut multiple layers depicted in the Helotes geologic framework model provide potential pathways for both vertical and lateral movement of water and hydraulic communication between aquifers. These fault surfaces along with localized zones of relatively intense small-scale faulting and extension fracturing, and limestone solution (karst conduit formation) provide likely communication pathways between the Edwards and Trinity Aquifers. The structural analyses presented in this report provide the basis for more detailed investigations of groundwater levels, multiwell pumping (drawdown) tests, tracer studies, and geochemical investigations to further investigate potential groundwater communication between the Edwards and Trinity Aquifers in the Helotes Quadrangle.

Acknowledgments

This work was funded jointly by the Edwards Aquifer Authority and the U.S. Army Corps of Engineers. We thank Steve Johnson, Geary Schindel and John Hoyt for their efforts in planning and executing the project. San Antonio Water System, Texas Bureau of Economic Geology, U.S. Geological Survey, and Edwards Aquifer Authority provided invaluable assistance. We especially thank Alvin Schultz for supplying well data and discussing interpretations in preparation for geologic framework modeling. We thank Allan Clark and Ted Small for an educational day in the field, and providing draft geologic mapping. Ranger Lionel Castillo and Reservoir Manager Tim A. Horn provided access to the Canyon Lake spillway discharge channel area and spillway gorge for research. Constructive reviews by Danielle Wyrick, Dr. H. Lawrence McKague, Dr. John Russell and Steve Johnson, and discussions with Dr. Gary Walter and Dr. Ronald Green improved this report. We thank Cheryl Patton for her assistance with report preparation.

TABLE OF CONTENTS

LIST OF FIGURES

Chapter 1:

Chapter 3:

Chapter 6:

Chapter 7:

LIST OF TABLES

1 INTRODUCTION

The Edwards and Trinity Aquifers are the primary sources of water for many south-central Texas communities, including the city of San Antonio (Figure 1-1). The Edwards Aquifer supplies residential water for 1.7 million people, serving as the primary source of water for San Antonio, and providing water for agriculture, industry, and recreation (Sharp and Banner, 1997; Hovorka et al., 1998; Johnson et al., 2002). Both aquifers are complex karst limestone aquifer systems that have permeability architectures that include a combination of host rock permeability, fractures and fault zones, and dissolution features. Although the strata that make up the Edwards Aquifer are younger and stratigraphically overlie the strata that comprise the Trinity Aquifer (Figure 1-2), displacement along faults of the Balcones fault system has placed the Edwards Aquifer laterally against (side-by-side with) the Trinity Aquifer. The location and amount of fault juxtaposition are sensitive to the location, geometry, and displacement on faults. Along faults that define the structural interface between the Edwards and Trinity Aquifers, caves and some fault zones provide conduits for groundwater flow and potential pathways for interaquifer communication. The occurrence of and degree to which interaquifer communication occurs is controversial and various hydrologic and geochemical studies have attempted to place constraints on the amount of water that the Trinity Aquifer contributes to the Edwards Aquifer.

The general question of the contribution of water from the Trinity Aquifer to the Edwards Aquifer is important as it pertains to both the quantity and quality of water in the Edwards Aquifer. If the Trinity Aquifer is hydraulically connected and provides water to the Edwards Aquifer, then the Edwards Aquifer recharge zone is in effect larger than the (Edwards) aquifer outcrop connected to the confined aquifer. In addition, the total dissolved solids content of Trinity Aquifer water is significantly higher than Edwards Aquifer water (LBG-Guyton Associates, 1995) and could potentially degrade the quality of the Edwards Aquifer. These issues of quantity and quality of water underlie the importance of understanding potential pathways for hydraulic communication between the Edwards and Trinity Aquifers. Recently the potential for interaquifer communication has received public attention in San Antonio due to the recognition and characterization of contamination of the Trinity Aquifer by pollutants from Camp Bullis (Needham, 2001a) and Camp Stanley (Needham, 2001b; Pearson and Murphy, 2004). Groundwater sampling studies on Camp Bullis have demonstrated southward movement of contaminants towards the Edwards Aquifer recharge zone and have drawn attention to the potential for contamination of the Edwards Aquifer by pollutants in the Trinity Aquifer (Needham, 2001a).

The purpose of the project reported here was to characterize the structural architecture of the Edwards and Trinity Aquifers for the area of the Helotes 7 ½ minute quadrangle (Figure 1-1). Included in this analysis were tasks to generate a three-dimensional computer model of the Edwards and Trinity Aquifer, and perform field investigations to characterize the mechanisms and products of localized fault-related deformation in the Edwards Aquifer and Trinity Aquifer near the study area. An important objective was to analyze the potential for communication between the Edwards Aquifer and the Trinity Aquifers, taking into account fault-related deformation and juxtaposition of the aquifers across key faults.
The project was organized into six tasks, including five technical tasks (summarized below), plus reporting:

1. 3DStress™ analysis to assess consistency of major faults in the context of the regional stress field at the time of faulting (Morris et al., 1996; Ferrill et al., 1999b).

2. Structural framework modeling (using EarthVision™) to define the 3-dimensional architecture of the study area.

3. Fault block deformation analysis based on assessment of displacement gradients on normal faults, which commonly produce locally intense fault block deformation (faults and fractures; Collins, 1993; Ferrill et al., 1999a), using the approach developed by Ferrill and Morris (2001).

4. Field analysis of fault zone materials and deformation mechanisms in accessible outcrops (primarily outside of the project study area) to determine parameters such as fault zone thicknesses, fault zone materials, and their distribution along faults with an emphasis on understanding the development of fault zone conduits (e.g., monoclines/synthetic dip panels, breccia zones, and dilatant damage zones; Caine et al., 1996; Ferrill and Morris, 2003) versus barriers (e.g., shale smear; Yielding et al., 1997).

5. Structural analysis of potential communication across the interface between the Edwards and Trinity Aquifers (Allan, 1989) taking into account four main considerations: geometry of stratigraphic horizons, fault displacement, fault geometry, and fault zone materials.

Results of the project show the aquifer architecture throughout the study area, the location and interpreted geometry of the most important mapped faults in the study area, and the deformation mechanisms and deformation style in fault zones in the rocks of both the Edwards and Trinity Aquifers. The three-dimensional geologic framework model of the Helotes area reveals
(i) juxtaposition of permeable and relatively impermeable hydrogeologic units, (ii) structural thinning of the Edwards and Trinity Aquifers, (iii) potential for cross-fault communication between the Edwards and Trinity Aquifers, (iv) faults expressed on the surface as potential infiltration pathways, and (v) maximum offset concentrated along a small number (two or three) fault systems (Maclay and Small, 1983; Maclay, 1995; Ferrill et al., 2003; Ferrill et al., 2004). This information, along with an understanding of fault zone deformation mechanisms and the role of fault zones as barriers or conduits, can assist in locating environmentally sensitive areas, is useful for aquifer flow path studies, and contributes to the identification of areas where communication between the Trinity and the Edwards Aquifers is suspected.

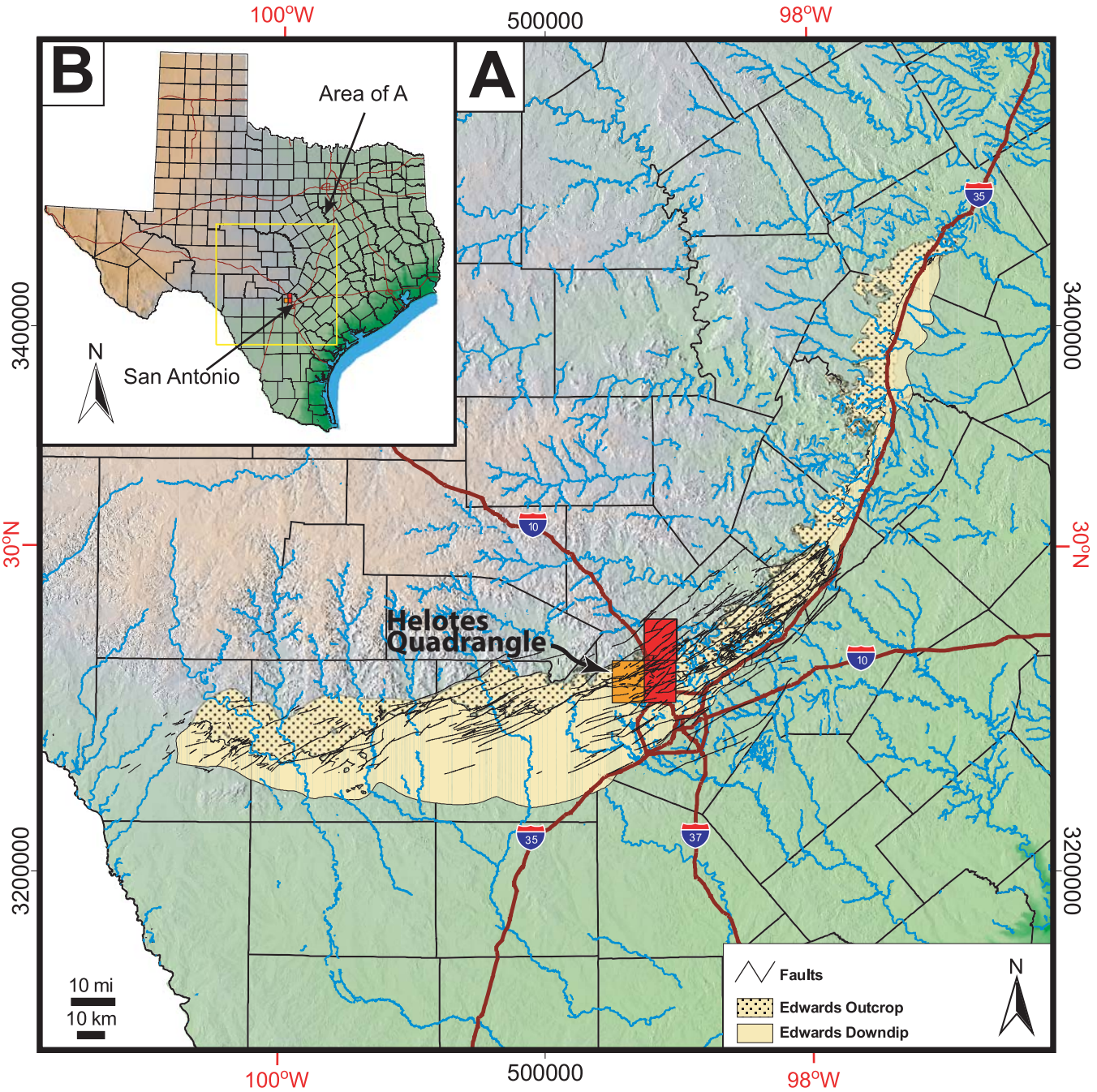

Figure 1-1. (A) Colored topography of south central Texas from 1°x1° tiles (Chalk Butte, Inc., 1994) showing counties, location of Edwards Aquifer (TNRIS, 1997), faults of the Balcones Fault zone (Collins and Hovorka, 1997), and location of model area. (B) Colored topography of Texas (Chalk Butte, Inc., 1994) showing the location of A. A and B base images were reprojected from geographic, decimal degrees to UTM, zone 14, meters.

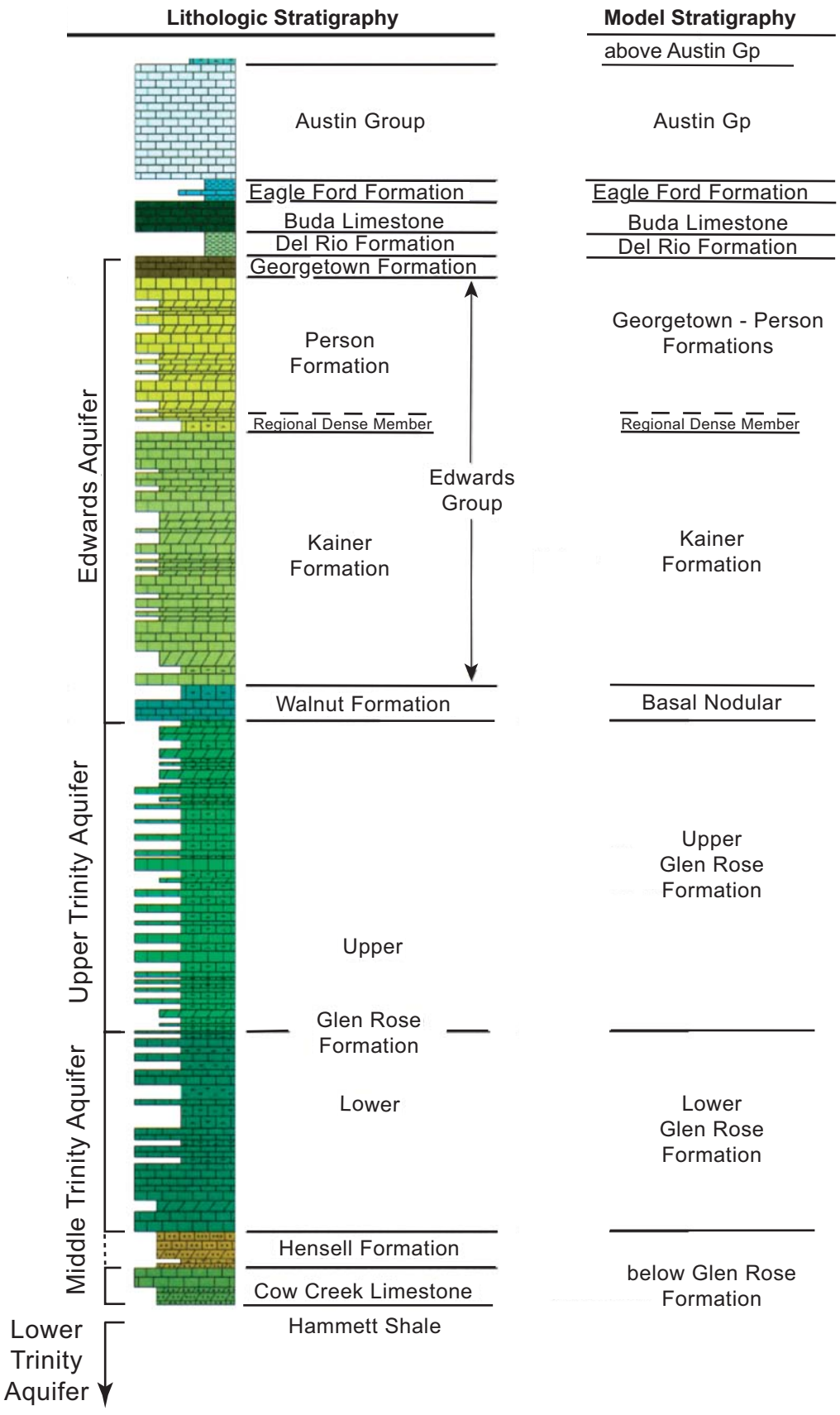

Figure 1-2. Stratigraphic column showing relationship between lithostratigraphic units and units used in the Helotes geologic framework model. Stratigraphic column is after Collins (2000).

2 BACKGROUND

The Edwards Aquifer is a karst aquifer (Maclay and Small, 1983; Johnson et al., 2002) consisting of porous, highly fractured lower Cretaceous limestone. Stratigraphically, the aquifer is in the Kainer and Person Formations of the Edwards Group and the overlying Georgetown Formation (Maclay and Small, 1983; Figure 1-2). The aquifer is constrained between an upper confining unit consisting of the Del Rio Clay, Buda Limestone, and Eagle Ford Formation and the underlying Upper Glen Rose Formation of the Trinity Group (Figure 1-2; Clark, 2000). The Trinity Aquifer consists of three parts: (i) the upper part consists of the Upper Member of the Glen Rose Formation, (ii) the middle part consists of the Lower Member of the Glen Rose Formation and the Cow Creek Limestone, which are separated by the Hensell Sand or Bexar Shale, and (iii) the lower part consists of the Hosston Formation and overlying Sligo Formation, and is separated from the Cow Creek Limestone by the intervening Hammett Shale (Mace et al., 2000).

The Trinity Aquifer extends across a wide region of the Texas Hill Country to the north and west of the main faults of the Balcones Fault System (Mace et al., 2000). The Edwards Aquifer extends along the Balcones Escarpment from Bell County in the north, curving southwestward through Williamson, Travis, Hays, Comal, Bexar, Medina, Uvalde, and Kinney Counties (TNRIS, 1997; Zahm et al., 1998; Hayes, 2000) (Figure 1-1). Although Trinity Aquifer strata are present beneath the Edwards Aquifer through the Balcones fault system, the Trinity is not considered to be a prolific groundwater producer in the area, and production is primarily from the Edwards. Exposures of the Edwards Aquifer strata along the Balcones Fault Zone represent the primary recharge zone, where surface water enters the Edwards Aquifer by way of fractures, faults, caves, sinking streams, and sinkholes (Maclay and Small, 1983, 1984; Maclay, 1995; Collins and Hovorka, 1997; Johnson et al., 2002). High porosity and permeability of the Edwards Aquifer allows for rapid recharge, but also creates opportunities for contamination of the aquifer with little filtration (Johnson et al., 2002). Subsurface flow paths in the Edwards Aquifer are thought to be controlled by structural architecture similar to fluid movement pathways in faulted oil fields (Ferrill et al., 2003; Ferrill et al., 2004).

Rocks of both the Edwards and Trinity Aquifers crop out in the Edwards Plateau region, and their southern and eastern outcrop boundary is within the Balcones Fault System, a zone of Tertiary age, down to the southeast, normal faulting (Foley, 1926; Maclay and Small, 1983, 1984; Stein and Ozuna, 1996; Clark, 2000; Collins, 2000). South and east of the Balcones Fault System, the Edwards Aquifer is confined beneath younger sedimentary rocks and serves as the primary water source for many communities, including the city of San Antonio. Recharge of the aquifer occurs primarily by streamflow loss and infiltration in porous parts of the unconfined Edwards Aquifer recharge zone, responding to rainfall in the recharge zone and upslope catchment area. Water in the unconfined aquifer moves down hydraulic gradient following, in many places, tortuous flow paths controlled by the Balcones Fault System. Natural discharge sites for the aquifer are springs associated with the Balcones Fault System in the vicinity of New Braunfels and San Marcos, Texas. Spring discharge in Bexar County is intermittent and feeds the San Antonio River through San Antonio Springs (Arnow, 1963). Most significant recharge of the aquifer occurs along the Balcones Fault System where faults, fractures, and solution-features such as sink holes and caves are considered to be major sites for groundwater recharge (Clark, 2000). By analogy with surface exposures, the high-volume, high flow-rate subsurface flow is also likely to be controlled primarily by faults, fractures, and solution cavities (Hovorka et al., 1998).

The Balcones Fault System is a broad *en echelon* system of mostly south-dipping normal faults that formed during the middle to late Tertiary (Murray, 1961; Young, 1972). The arcuate zone trends east-

northeast and spans much of central Texas. The 25 to 30 km (16 to 19 mi) wide Balcones Fault System has a maximum total displacement of about 366 m (1201 ft) (Weeks, 1945), and defines the transition from structurally stable flat-lying rocks of the Texas craton to gently coastward-dipping sediments of the subsiding Gulf of Mexico. At the margin of the Texas Hill Country northwest of San Antonio, exposures in Cretaceous-aged platform carbonates include the Edwards Group, a series of carbonate strata that formed along the margin of the Central Texas platform with the ancestral Gulf of Mexico (Rose, 1972). Offset of carbonate strata across the Balcones Fault System resulted in a broad, weathered escarpment of vegetated limestone hills rising from the predominantly clastic coastal plains to the uplands of the Texas Craton. Within the fault system, the dip of bedding varies from gentle coastward dips to nearly horizontal, with occasional localized dip of hanging wall beds northward into some faults. Faulting has been interpreted as being rooted in the deeply buried foreland-basin sediments of the Ouachita orogeny (Murray, 1956).

A primary control on the permeability architecture of stratified rocks is the difference in permeability between rock layers. If a stratigraphic sequence is not deformed, this vertical inhomogeneity and anisotropy produced by layering will dominate bulk permeability. In faulted strata, however, geologic structures (faults and fractures) exert three additional controls on aquifer permeability and flow:

1. Fault offsets alter the overall geometry and thickness of aquifer strata and communication between aquifer strata in different fault blocks (Allan, 1989; Maclay, 1989; Ferrill and Morris, 2001).

2. Fault zones commonly form relatively impermeable barriers to across-fault flow, form permeable pathways for along-fault flow, or form both barriers and pathways (Arnow, 1963; Caine et al., 1996; Knipe, 1997; Yielding et al., 1997; Ferrill and Morris, 2003). This fault and fracture conductivity may be influenced by the current stress field and fault activity (Finkbeiner et al., 1997; Ferrill et al., 1999b).

3. Fault block deformation by formation of small faults and fractures leads to permeability anisotropy (Antonellini and Aydin, 1994; Mayer and Sharp, 1998; Ferrill et al., 2000).

These three controls are listed in generally descending order of scale of influence from regional, to subregional, to local. In carbonate rock layers like those that make up the Edwards and Trinity groundwater flow and associated limestone dissolution (Deike, 1990) can enhance the permeability effects of fault and fracture systems, producing solution enlargement at scales of individual fractures to cave networks consisting of fissures, angular passages, and fracture controlled networks of passages (Palmer, 1991; Loucks, 1999). Alignment of linear cave segments and cave networks with fracture patterns, and direct observation of association of caves with faults and fractures, indicate that fault and fracture control is common for caves in the Edwards Aquifer recharge zone (Wermund and Cepeda, 1977; Wermund et al., 1978; Kastning, 1981; Hovorka et al., 2004). Modification of faults and fractures by dissolution were thought to produce some of the most important paths for recharge of the Edwards Aquifer (Clark, 2000).

Geologic structures in the Edwards and Trinity Aquifers influence permeability architecture at a range of scales (Ferrill et al., 2003; Ferrill et al., 2004). At a regional scale, the influence of faults and fractures on the aquifer could be described using one or more permeability tensors. Although not typically incorporated into groundwater flow simulations of the Edwards and Trinity Aquifers, structurally controlled permeability anisotropy has been incorporated with greater hydraulic conductivity parallel to

faulting, and less perpendicular to faulting (Kuniansky and Holligan, 1994). At the scale of individual recharge features, flow conduits causing significant heterogeneity are observed. Here we consider the scale range from regional flow models down to that of individual recharge features, flow conduits, and wells. Structural control on permeability architecture can be subdivided into three components (Ferrill et al., 2004). At the largest scale, major faults of the Balcones Fault System control the overall geometry of the aquifer, including its position at the ground surface (recharge zone), dip magnitude (angle) and direction, and position of the aquifer in the subsurface. Major faults produce tilting of fault blocks and locally thin the aquifer to some fraction of its original thickness or in some cases completely offset the aquifer. Thus, aquifer communication may be decreased or lost entirely in directions perpendicular to the fault strike because of thinning. Fault zones themselves generally have increased permeability parallel to the fault zone, and relatively reduced permeability perpendicular to the faults. These faults locally serve as conduits for vertical and lateral water movement. Smaller faults and extension fractures within fault blocks produce permeability anisotropy within fault blocks. Fault block deformation by small-scale faulting and extension fracturing is heterogeneously developed within the Edwards Aquifer. High intensities of small faults occur close to large faults (within ~100 m, ~328 ft). In the Edwards Aquifer, the role of major faults for geometry and thinning of the aquifer has been identified (Maclay and Small, 1983; Hovorka et al., 1998; Collins, 2000), as has the importance of individual faults as infiltration and subsurface flow pathways (Clark, 2000; Ferrill and Morris, 2003). The role of fault block deformation in the Edwards Aquifer is variable, and is controlled primarily by structural position, specifically, proximity to large (>10 m (33 ft) maximum displacement) faults.

An important question with respect to the Edwards Aquifer recharge zone, and related subsurface groundwater flow in the confined Edwards Aquifer, is whether there is subsurface flow communication (i) across faults within the Edwards Aquifer, (ii) between the Edwards Aquifer, Buda Limestone, and Austin Chalk, higher in the stratigraphic section, or (iii) between the Edwards Aquifer and the Glen Rose Formation (Trinity Aquifer) below. Such flow communication could be the result of flow across faults, flow laterally or vertically within a fault zone, or a combination of these. Water that infiltrates in other stratigraphic units may be capable of flowing laterally into the Edwards Aquifer. This potential for subsurface aquifer communication is important because it controls the amount and distribution of areas that provide recharge to the Edwards Aquifer, thereby effectively expanding the recharge zone. In addition, communication between aquifers could mean increased threat for either lower quality water or contaminant migration into the Edwards Aquifer from other aquifers such as the Trinity Aquifer.

Faults that juxtapose the Edwards Aquifer with itself are not likely to be effective barriers to across-fault aquifer communication, because the Edwards Aquifer stratigraphic section does not contain significant clay-rich sealing layers. Field observations, in particular the common occurrence of dissolution enlargement of faults, suggest that fault zone deformation processes in these limestones more commonly enhance rather than reduce permeability. Structural thinning of the aquifer by normal faults does, however, constrict flow/communication pathways (Maclay and Small, 1983). Continuous monitoring of water table elevations in the Edwards Aquifer recharge zone suggests that there is local reduction in hydraulic communication across some faults within the Edwards (Steve Johnson, Edwards Aquifer Authority, personal communication). This observation warrants further structural and hydrologic investigations.

The Del Rio Formation introduces a very effective barrier to aquifer communication across faults, even in cases where fault displacement is greater than the thickness of the Del Rio Formation (Ferrill et al., 2004). The mechanically weak character of the clay rich Del Rio Formation may allow it to smear along fault planes, resulting in a barrier to across-fault water movement. In the same way, shale of the Eagle Ford

Formation is likely to remain an effective barrier to communication between the limestones of the Austin Group and the Buda Limestone and Edwards Group limestones beneath. However, the presence of springs (e.g., San Antonio and San Pedro Springs; Ferrill et al., 2004) that discharge water from the Edwards Aquifer in the outcrop area of the Austin Chalk and Pecan Gap Chalk, both stratigraphically above the Eagle Ford Formation, implies that faulting in these localities has breached the clay smear seal.

In contrast, across-fault communication between the Edwards Group limestones and underlying limestones of the Trinity Aquifer's Glen Rose Formation is likely. Although argillaceous limestones are present intermittently throughout the Glen Rose Formation, there is no clay-rich shale separating the Edwards Group from the underlying Trinity Aquifer rocks that would retard fault propagation as successfully as the Del Rio Formation. For this reason, the potential for aquifer communication between the Glen Rose Formation (Trinity Aquifer) and Edwards Aquifer warrants further analysis. This is of great importance because the Glen Rose Formation crops out over a very large area adjacent to and north of the Edwards Aquifer recharge zone along the Balcones Fault System. If water from the Glen Rose Formation feeds into the Edwards Aquifer along subsurface flow pathways, then the Edwards Aquifer recharge zone is in effect larger than currently described and modeled. Also, groundwater contamination north of the Edwards Aquifer recharge zone may be a threat to water quality in the Edwards Aquifer. Additional structural characterization, coupled with water table characterization, pump testing, and natural and induced tracer tests, is needed to further evaluate the potential for subsurface aquifer communication.

3 AQUIFER ARCHITECTURE

We constructed a three-dimensional digital geologic framework model of the Helotes Quadrangle, including a portion of the interface between the rocks of the upper and middle Trinity Aquifer and Edwards Aquifer using EarthVision 6.1 (Dynamic Graphics, 2001; Figures 3-1 through 3-14). The model was constructed with goals of producing a three-dimensional representation of the faulted aquifers and confining strata that can be used to determine and illustrate potential structural controls upon recharge and groundwater flow and transmissivity within or between the Edwards and Trinity Aquifers in the Helotes Quadrangle.

3.1 Methodology

We followed the approach for model construction that we previously developed in producing the three-dimensional geologic framework model of the Castle Hills and Camp Bullis quadrangles, immediately to the east and northeast of the area of this study (Ferrill et al., 2003; Waiting et al., 2003; Ferrill et al., 2004). The workflow for model construction is summarized below. For a thorough discussion of the workflow for three-dimensional geologic framework model construction, see Waiting et al. (2003).

3.1.1 Data

Construction of a three-dimensional geologic framework model requires data in sufficient quantity to cover as much of the model area as possible. In the case of the Helotes model, this includes both surface and subsurface data.

Acquisition of surface data for this project began with downloading United States Geological Survey (USGS) 30-meter horizontal resolution Digital Elevation Models (DEMs) from the Texas Natural Resources Information System website. This supplied surface elevations for the area of the model.

The USGS supplied vector coverages of faults digitized from published hydrogeologic maps of the Edwards Aquifer for Bexar, Comal, Hays, and Medina Counties (Small and Hanson, 1994; Hanson and Small, 1995; Stein and Ozuna, 1996; Small and Clark, 2000). The Texas Bureau of Economic Geology made available digital coverages from the 30′ x 60′ New Braunfels, Texas Geologic Quadrangle map, which is comparable in area to thirty-two (32) 7 ½ minute quadrangles (Collins, 2000). This information provided the mapped surface geology, including faults, for comparison with other interpretations.

Surface data included field observations from exposures of the Glen Rose Formation and Edwards Group and overlying layers in roadcuts and quarries. Subsurface data provide important constraints for a three-dimensional geologic framework model to correctly represent the bedding thickness and bedding orientation, as well as constrain the geometry of model horizons. Subsurface data also verify surface data and provide fault dips at depth, as well as fault throw. San Antonio Water System (SAWS) and Mr. Alvin Schultz (a consultant with San Antonio Water System) provided a database file containing the elevations of the tops of the stratigraphic units from interpreted geophysical logs for 102 wells located in the Helotes Quadrangle.

3.1.2 Map Projection

In a digital three-dimensional geologic framework model, geologic structures are constructed as a system of geometric elements. In the case of the model of the Helotes Quadrangle, these elements include

stratigraphic horizons represented as volumes having upper and lower bounding surfaces terminated either by fault surfaces or model boundaries. To reasonably replicate the spatial and angular relationships between the natural geologic features and model elements, it is necessary that the map projection be both equal area and equal angle, and that the horizontal and vertical units are similar. Universal Transverse Mercator meets these requirements, and is widely used in the geologic and hydrologic communities. We used the Universal Transverse Mercator (UTM, NAD27) coordinate system.

3.2 Results

The model covers the area outlined by the USGS 7 ½ minute 1:24,000 Helotes Quadrangle (for example USGS 7.5 minute series topographic map of Helotes Quadrangle, Texas—Bexar Co., 1992; approximately 1.68 x10^8 m^2 or 1.8 × 10^9 ft^2) (Figures 1-1 and 3-1). The model volume is 1.35 ×10^{11} m^3 (4.8 × 10^{12} ft^3), its upper boundary is the topographic surface (maximum elevation 488 m (1601 ft) and minimum elevation 61 m (200 ft)), and it extends to a depth of 100 m (328 ft) below mean sea level. USGS 30 m (98 ft) digital elevation data in DEM format were used to construct the topographic surface.

Twelve stratigraphic horizons present in outcrop or in the subsurface are represented in the model volume. The stratigraphic horizons are selected for hydrogeologic associations (Figure 1-2) and for characteristic outcrop or geophysical log signatures, and represent both aquifer and confining strata. Represented in the model are portions of the unconfined Edwards Aquifer, and the upper and middle Trinity Aquifers. Model horizon designations, from oldest to youngest, are 'below Glen Rose Fm' (Figure 3-2), 'Lower Glen Rose Fm' (Figure 3-3), 'Upper Glen Rose Fm.' (Figure 3-4), 'Basal Nodular mbr' (Figure 3-5), 'Kainer Fm' (exclusive of Basal Nodular member; Figure 3-6), 'Regional Dense mbr' (basal part of Person Formation; Figure 3-7), 'Georgetown-Person Fms' (exclusive of Regional Dense member of the Person Formation; Figure 3-8), 'Del Rio Fm' (Figure 3-9), 'Buda Fm' (Figure 3-10), 'Eagle Ford Fm' (Figure 3-11), 'Austin Gp' (Figure 3-12), and 'above Austin Gp' (Figure 3-13).

Structure in the model is constrained using published (Arnow, 1963; Reeves, 1972; Small and Hanson, 1994; Hanson and Small, 1995; Groshen, 1996; Stein and Ozuna 1996; Collins and Hovorka, 1997, Mace et al., 2000, and Collins, 2000) and unpublished (Alvin Schultz, consultant to San Antonio Water System, San Antonio, Texas, 78298) maps, cross-sections and subsurface data, results from field investigations, and unpublished interpreted geophysical well logs (Alvin Schultz, consultant to San Antonio Water System, San Antonio, Texas, 78298). Lithologies exposed in the area consist of a thick sequence of faulted carbonate layers that can be difficult to differentiate. As a result, published geologic and hydrogeologic maps of the Balcones escarpment do not show uniform interpretations of fault traces or surface outcrops. Collaboration between Alvin Schultz, Edwards Aquifer Authority personnel and the authors of this report resulted in the formulation of a set of criteria by which to reconcile the different interpretations. Faults from published maps are generally included in the model where: (i) the fault is included and congruent in all interpretations, (ii) the fault is included on one or more maps and is required to reconcile outcrop or subsurface data, (iii) the fault shows vertical offset greater than 5 m (16 ft), or (iv) the fault is included on one or more maps and is geometrically reasonable relative to the fault system. The selection of 5 m (16 ft) as the threshold vertical displacement for inclusion in the model is based on the ambiguity and inconsistency in regional mapping of faults smaller than this based on uncertain field and wellbore data. Faults from published maps are generally excluded where: (i) maximum vertical displacement is less than 5 m (16 ft), (ii) the fault is clearly in conflict with outcrop or subsurface data, or (iii) the fault is not required to accommodate horizon or fault system geometry. The selection of faults was refined and supported unpublished (Alvin Schultz, consultant to San Antonio Water System, San Antonio, Texas, 78298) interpretations of geophysical well logs.

While relative displacement or dip direction is indicated on some published maps and cross-sections (Stein and Ozuna, 1996; Collins and Hovorka, 1997; Collins, 2000), few data were available to constrain subsurface geometry of individual faults. A few fault systems are locally exposed in quarries or roadcuts. Where present, slip indicators on these exposed fault surfaces show predominant normal dip-slip displacement. In the model, fault dip direction was generally constrained by assuming that the displacement of stratigraphic horizons resulted from normal dip-slip displacement. Dip magnitude was constrained generally by tabulating fault geometries exposed in roadcuts, and computing an average fault dip for the dominant stratigraphic package, the Glen Rose Formation (Ferrill et al., 2004). In the model, faults exposed in the Edwards outcrop area have dips of 75°, and those exposed in the Glen Rose outcrop area have dips of 60°. Field observations of fault systems exposed in quarry walls and roadcuts indicate that fault zones can be simple to complex, and that fault zone deformation is strongly controlled by characteristics of the host strata (discussed in detail in section 5). In most cases, individual faults within fault zones are below the scale of the geologic framework model, and fault zones are represented in the model as single surfaces that accommodate all indicated displacement.

Bedding geometry in the model is constrained by map, outcrop, and subsurface data. Regional dip of bedding in the area is gentle (<1°) and towards the southeast. Tilting of faulted blocks is generally slight to undetectable, with the occasional exception of localized low-angle antithetic dip (opposite direction to fault dip) of bedding (Collins, 1993), or synthetic dip (in the same direction as the fault dip; e.g., Ferrill et al., 2005) seen in monoclines above fault tips (fault terminations) and in faulted monoclines. Steep bedding dip associated with displacement transfer zones between overlapping fault segments is not generally observed (Collins, 1993). Outcrop geometry in the model is constrained by both subsurface (wellbore) data and mapped bedding traces. It is possible to force outcrop patterns in three-dimensional visualization models to match those of two-dimensional maps. However, as the interpretation is an amalgam that includes other interpretations, the outcrop trace of bedding in the model will not necessarily duplicate any one published map, but may instead highlight regions that are potentially misinterpreted or mis-recorded in previous work. Also, although the digital representation of the topography is reasonably detailed, vertical control of the digital elevation data is not sufficient across the model to warrant detailed forcing of outcrop patterns.

Our three-dimensional geologic framework model of the geology of the Helotes area was constructed using a reference-isochore method. In this approach a reference horizon is constructed using outcrop, fault, and subsurface data. South of the Haby Crossing fault, the top of the Georgetown Formation was used as the control surface for model construction, based on the availability of well data and geologic mapping control. North of the Haby Crossing fault, the top of the Upper Glen Rose Formation was used as the control surface, and was constructed based on a combination of well data and surface geologic mapping. Based on an assumed uniform thickness for the Edwards Aquifer (153.2 m, 503 ft) and the 3D control surface for the top of the Upper Glen Rose, the top of Edwards horizon was projected northward to extend across the entire Helotes Quadrangle model area as a reference horizon. Upon completion of the reference horizon, model horizons above and below the top-Georgetown reference horizon were projected using stratal thicknesses. Thickness variations are reported for each of the lithostratigraphic horizons represented in the model (Arnow, 1963; Maclay and Rettman, 1972; Ashworth, 1983; Maclay and Small, 1976, 1983; Shaw, 1978; Small, 1984, 1985; Waterreus, 1992; Barker et al., 1994; Collins, 2000; Mace et al., 2000; Alvin Schultz, Consultant, San Antonio Water System, San Antonio, Texas, 78298). Sufficient data are available to incorporate local thickness variation into the twelve model horizons (Table 3-1, Figures 3-2 through 3-13). In each of these horizons, thickness is calculated from wellbore thickness data using minimum tension gridding. Minimum tension grids such as those produced using EarthVision (Dynamic Graphics, 2001) are formed by calculating a non-linear interpolation

between adjacent nodes, where surface curvature is distributed between grid nodes rather than concentrated at grid nodes. The resulting surface gives a reasonable approximation of the geologic layer surfaces commonly observed in nature.

The twelve horizons in the geologic framework model are offset by 30 faults. Dominant fault trace orientation is northeast–southwest, and dip is predominantly to the southeast. Faults are distributed across the model; however, the Haby Crossing fault which traverses the model from west-southwest to east–northeast, accommodates between 30 percent and 50 percent of the total throw of the Balcones Fault system in the Helotes area. Many faults intersect with other faults at one or both ends, or are artificially truncated by the model boundaries. Vertical offset (throw) ranges from near zero to an approximate maximum of 178 meters (584 ft). Displacement sense is normal, and commonly down to the southeast, although there are five faults south of the Haby Crossing fault with significant (as much as 65 m, 213 ft) down-to-the north-northwest throw. Both half-graben systems and full-graben systems are present. Maximum offset is concentrated along two down-to-the-south fault systems: the Haby Crossing fault and the Diversion Lake fault (Figures 3-2 to 3-5). The Haby Crossing fault is the principal fault within the Balcones Fault Zone in this area and juxtaposes at least 68 percent of the Edwards Group stratigraphic thickness with rocks of the Glen Rose Formation across the entire model area. Displacement gradients are generally small, including where faults have isolated tips, although the Haby Crossing fault in the vicinity of the City of Helotes is interpreted to have throw gradients as high as 0.03. In map view, fault blocks are elongate, with the long axis oriented northeast–southwest. Block tilting is not remarkable, but can be detected in some blocks.

TABLE 3-1. MODEL HORIZON THICKNESSES

Model horizon name	Min. thickness	Max. thickness	Mean thickness
above Austin Gp	N.A.	N.A.	N.A.
Austin Gp	31.7 (104.0 ft)	46.5 (152.6 ft)	42.5 (139.4 ft)
Eagle Ford Fm	4.7 (15.4 ft)	13.2 (43.3 ft)	9.9 (32.5 ft)
Buda Fm	10.0 (32.8 ft)	19.9 (65.3 ft)	14.8 (48.6 ft)
Del Rio Fm	11.6 (38.1 ft)	21.9 (71.8 ft)	16.0 (52.5 ft)
Georgetown-Person Fms	41.7 (136.8 ft)	68.4 (224.4 ft)	55.1 (180.8 ft)
Regional Dense mbr	5.4 (17.7 ft)	9.5 (31.2 ft)	6.3 (20.7 ft)
Kainer Fm	69.3 (227.4 ft)	85.9 (281.8 ft)	75.8 (248.7 ft)
Basal Nodular mbr	12.8 (42.0 ft)	19.7 (64.6 ft)	16.9 (54.4 ft)
Upper Glen Rose Fm	141.7 (464.9 ft)	148.5 (487.2 ft)	146.0 (479.0 ft)
Lower Glen Rose Fm	N.A.	N.A.	100.3 (329.1 ft)
below Glen Rose Fm	N.A.	N.A.	N.A.

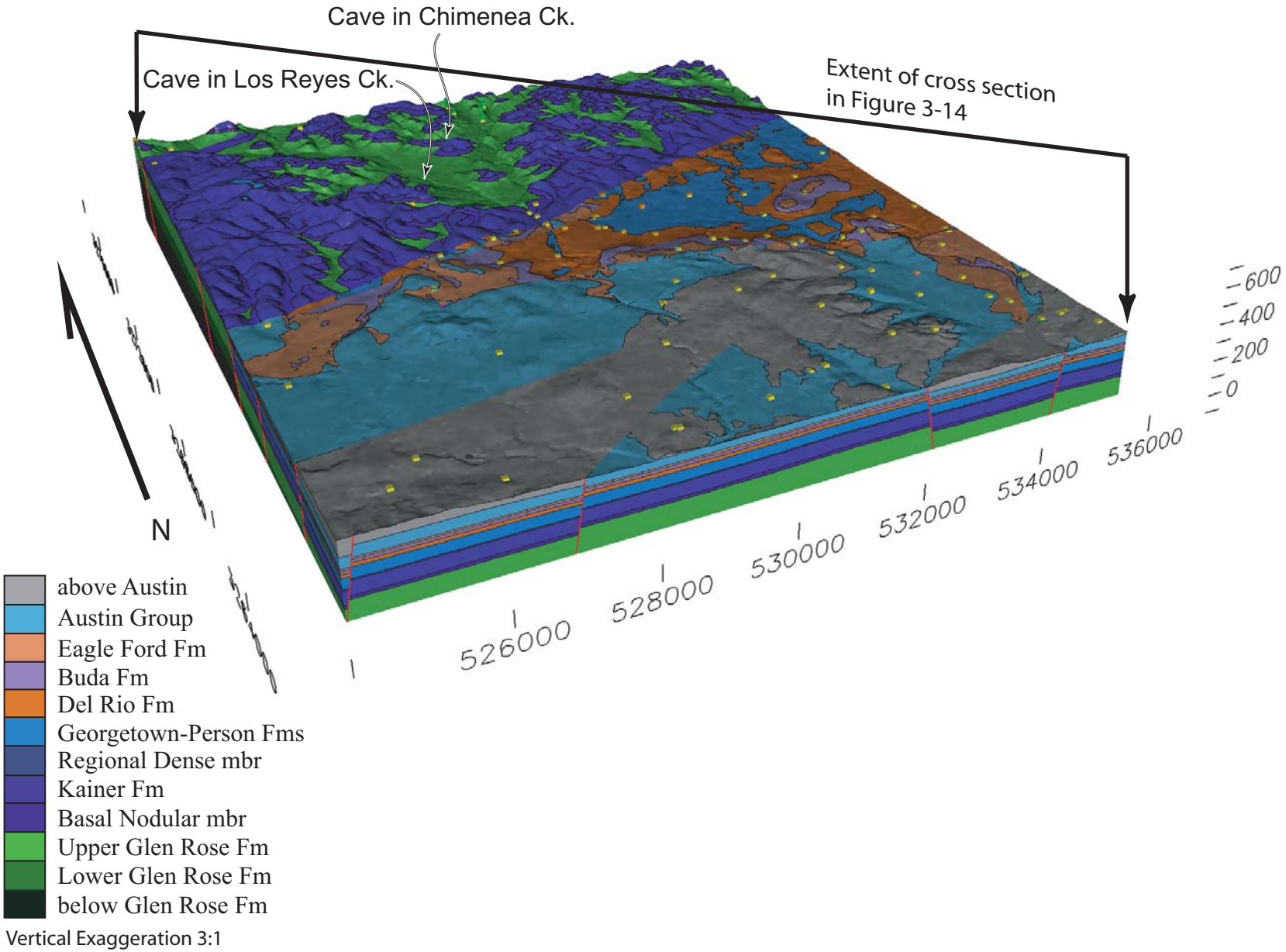

Figure 3-1. Oblique view of the Helotes geologic framework model. Coordinates are UTM meters, NAD27. View direction is NE. Illumination from SW. Yellow points show well locations.

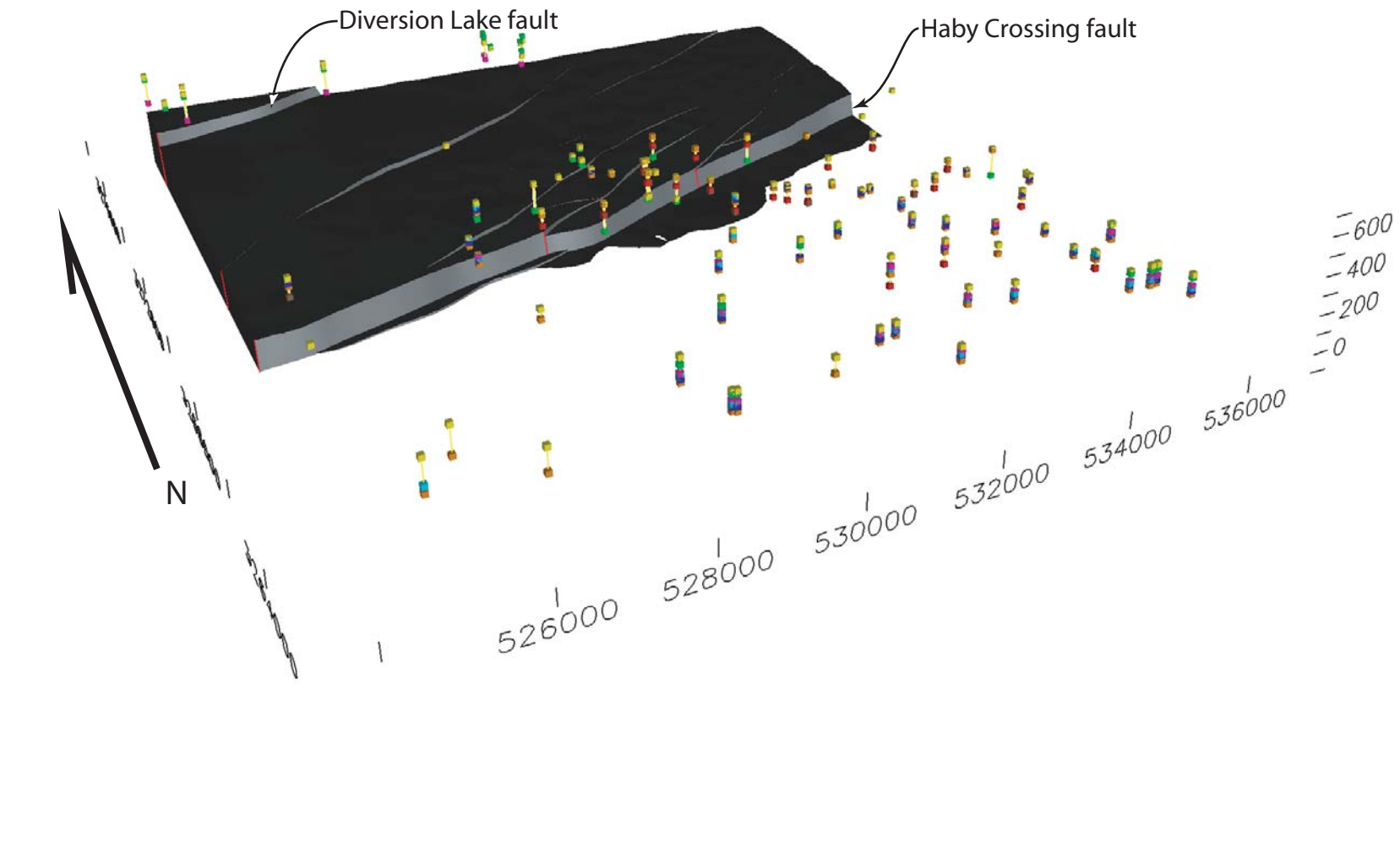

Figure 3-2. Oblique view of the Helotes geologic framework model horizon ‘below Glen Rose Fm'. Coordinates are UTM meters, NAD27. View direction is NE. Illumination from SW. Yellow points show well locations at land surface, and other points on well bores are stratigraphic picks that can be queried in the geologic framework model.

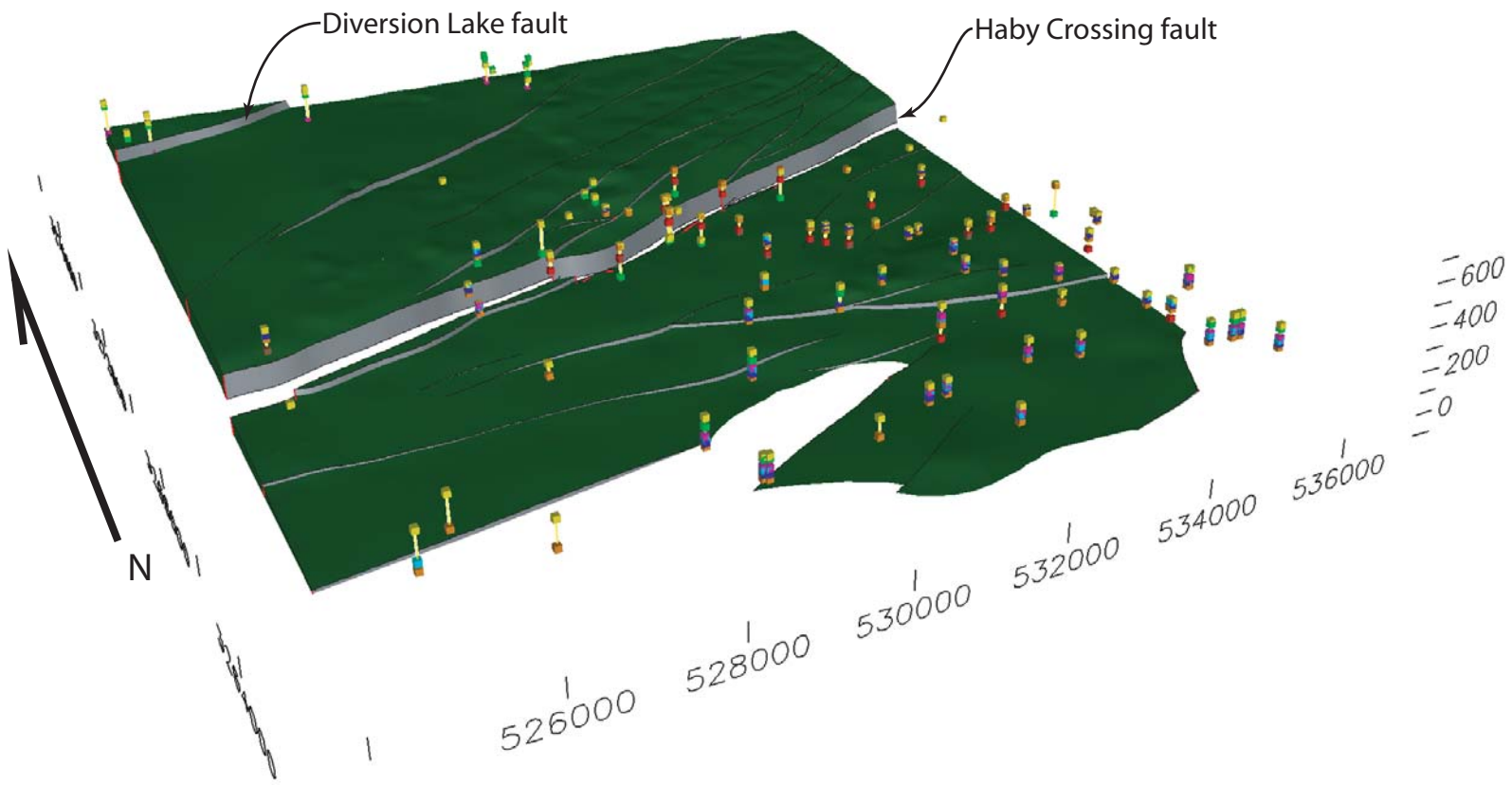

Figure 3-3. Oblique view of the Helotes geologic framework model horizon 'Lower Glen Rose Fm'. Coordinates are UTM meters, NAD27. View direction is NE. Illumination from SW. Yellow points show well locations at land surface, and other points on well bores are stratigraphic picks that can be queried in the geologic framework model.

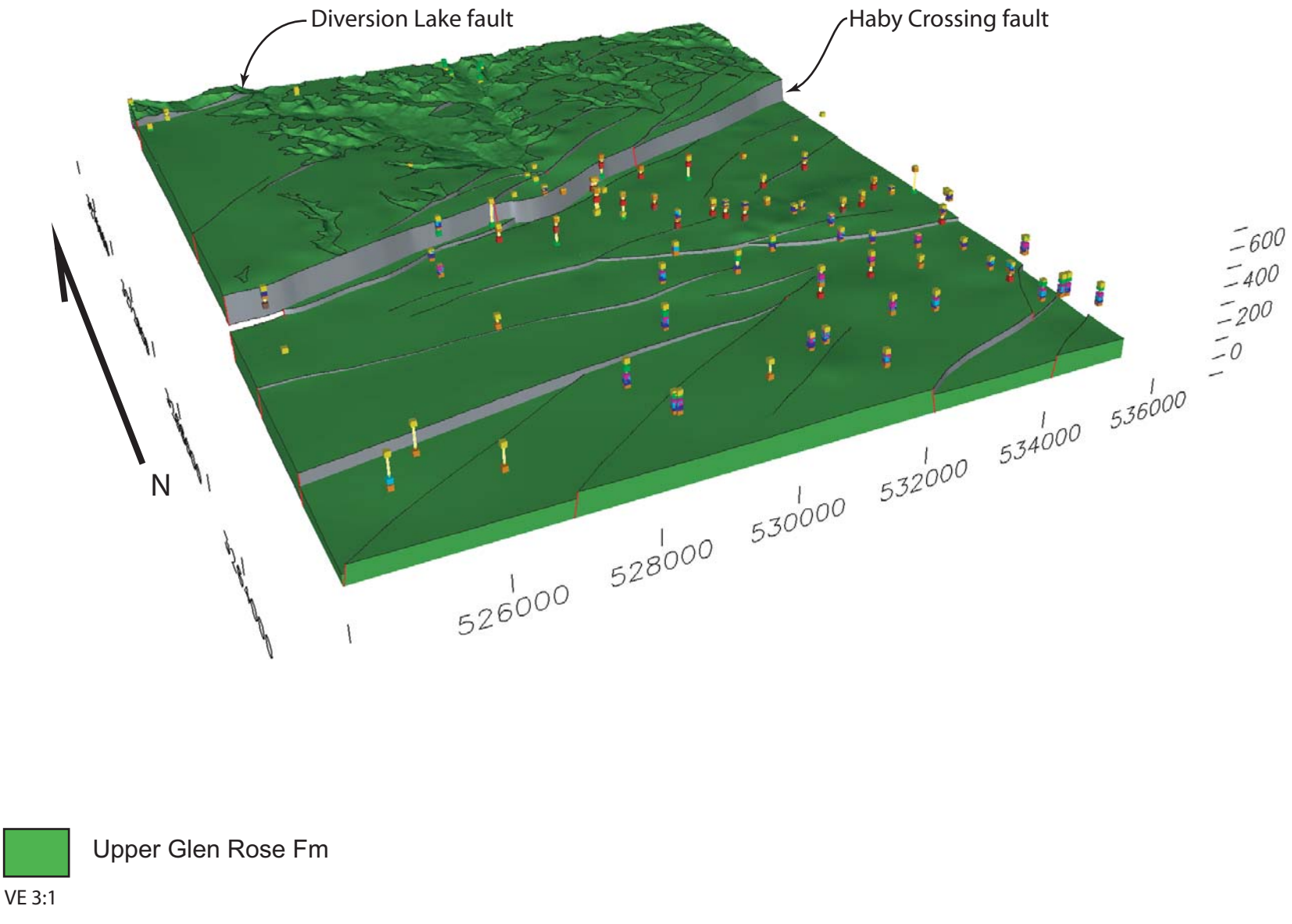

Figure 3-4. Oblique view of Helotes geologic framework model horizon ‘Upper Glen Rose Fm'. Coordinates are UTM meters, NAD27. View direction is NE. Illumination from SW. Yellow points show well locations at land surface, and other points on well bores are stratigraphic picks that can be queried in the geologic framework model.

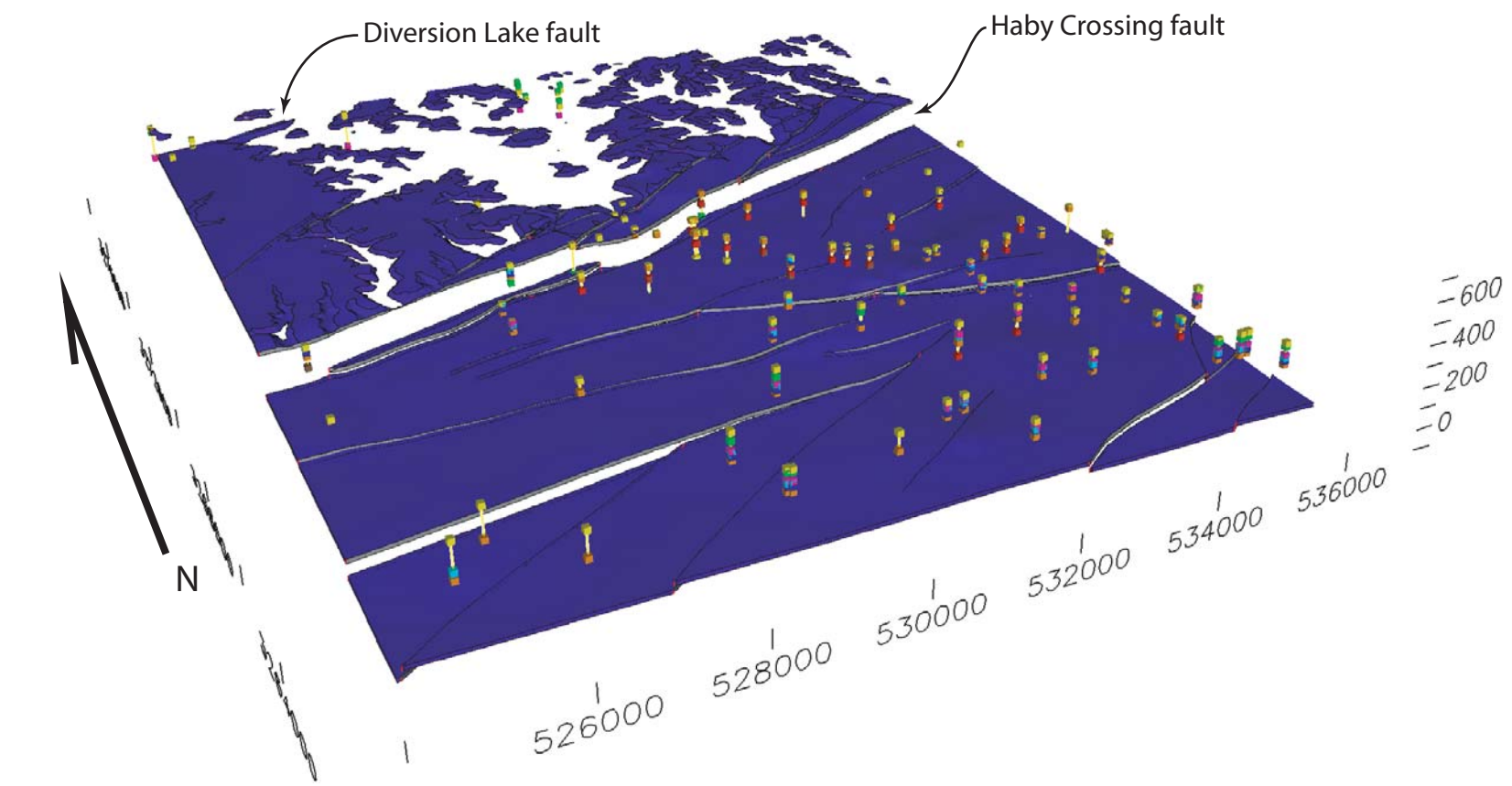

Figure 3-5. Oblique view of the Helotes geologic framework model horizon 'Basal Nodular mbr'. Coordinates are UTM meters, NAD27. View direction is NE. Illumination from SW. Yellow points show well locations at land surface, and other points on well bores are stratigraphic picks that can be queried in the geologic framework model.

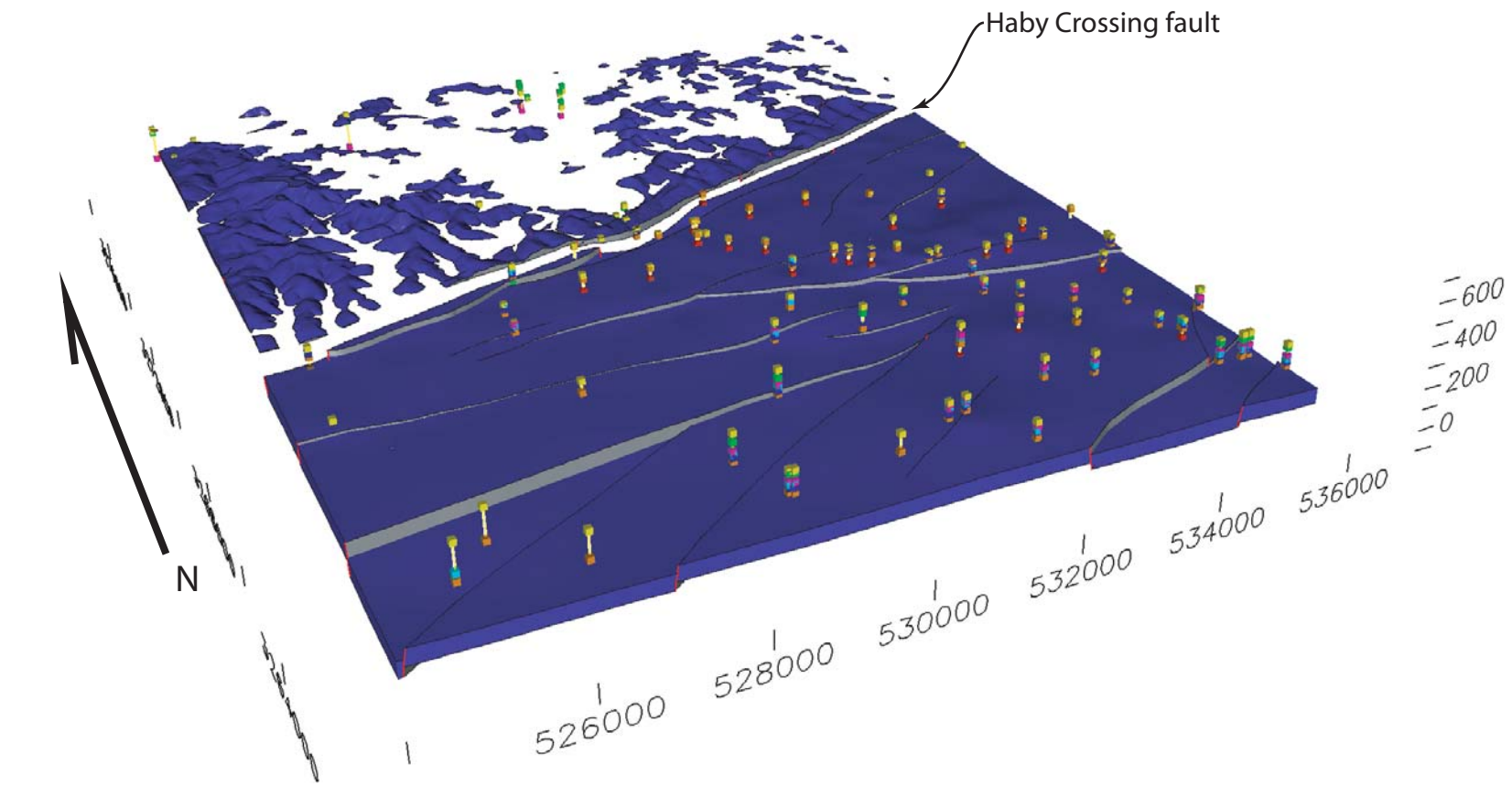

Figure 3-6. Oblique view of the Helotes geologic framework model horizon 'Kainer Fm'. Coordinates are UTM meters, NAD27. View direction is NE. Illumination from SW. Yellow points show well locations at land surface, and other points on well bores are stratigraphic picks that can be queried in the geologic framework model.

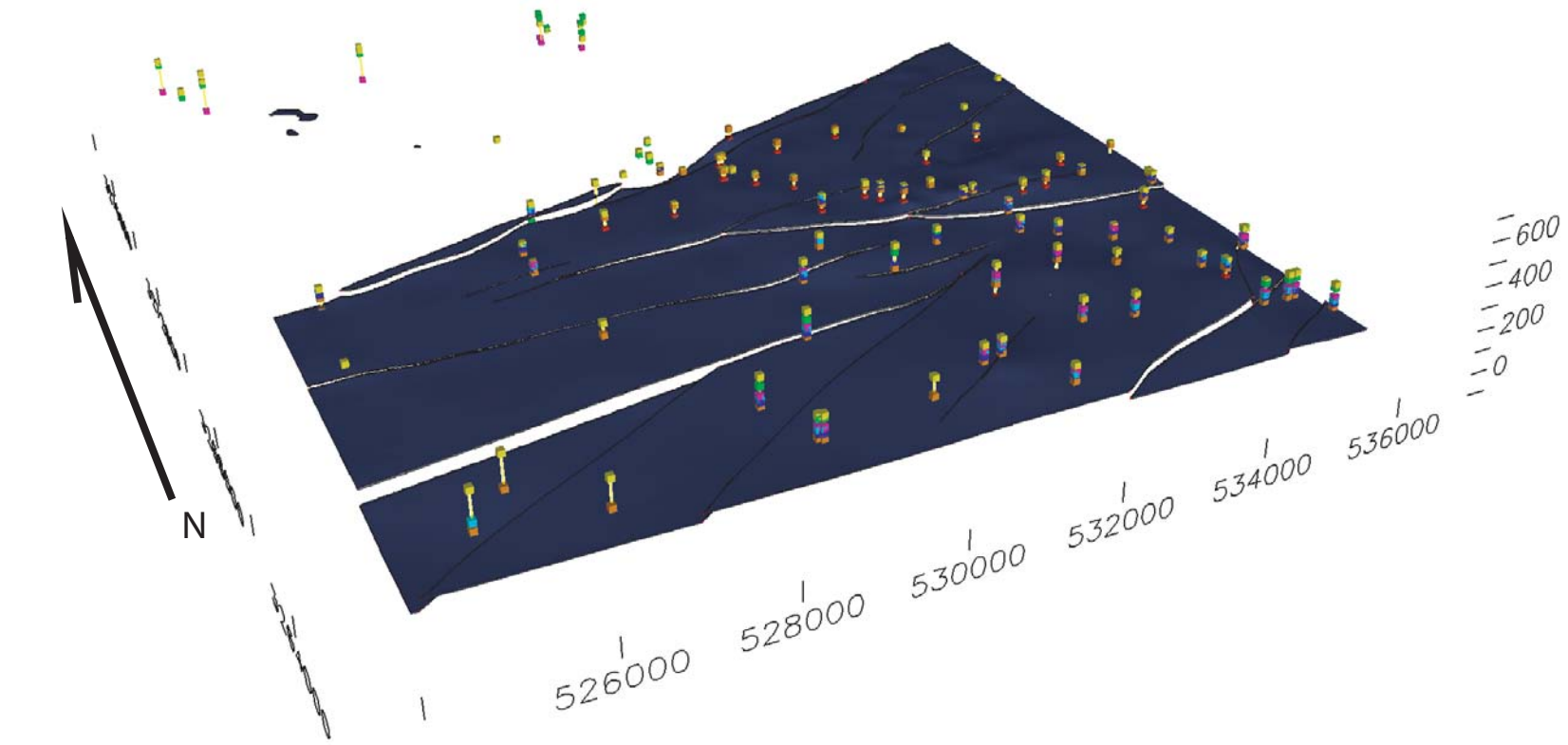

Figure 3-7. Oblique view of the Helotes geologic framework model horizon ‘Regional Dense mbr'. Coordinates are UTM meters, NAD27. View direction is NE. Illumination from SW. Yellow points show well locations at land surface, and other points on well bores are stratigraphic picks that can be queried in the geologic framework model.

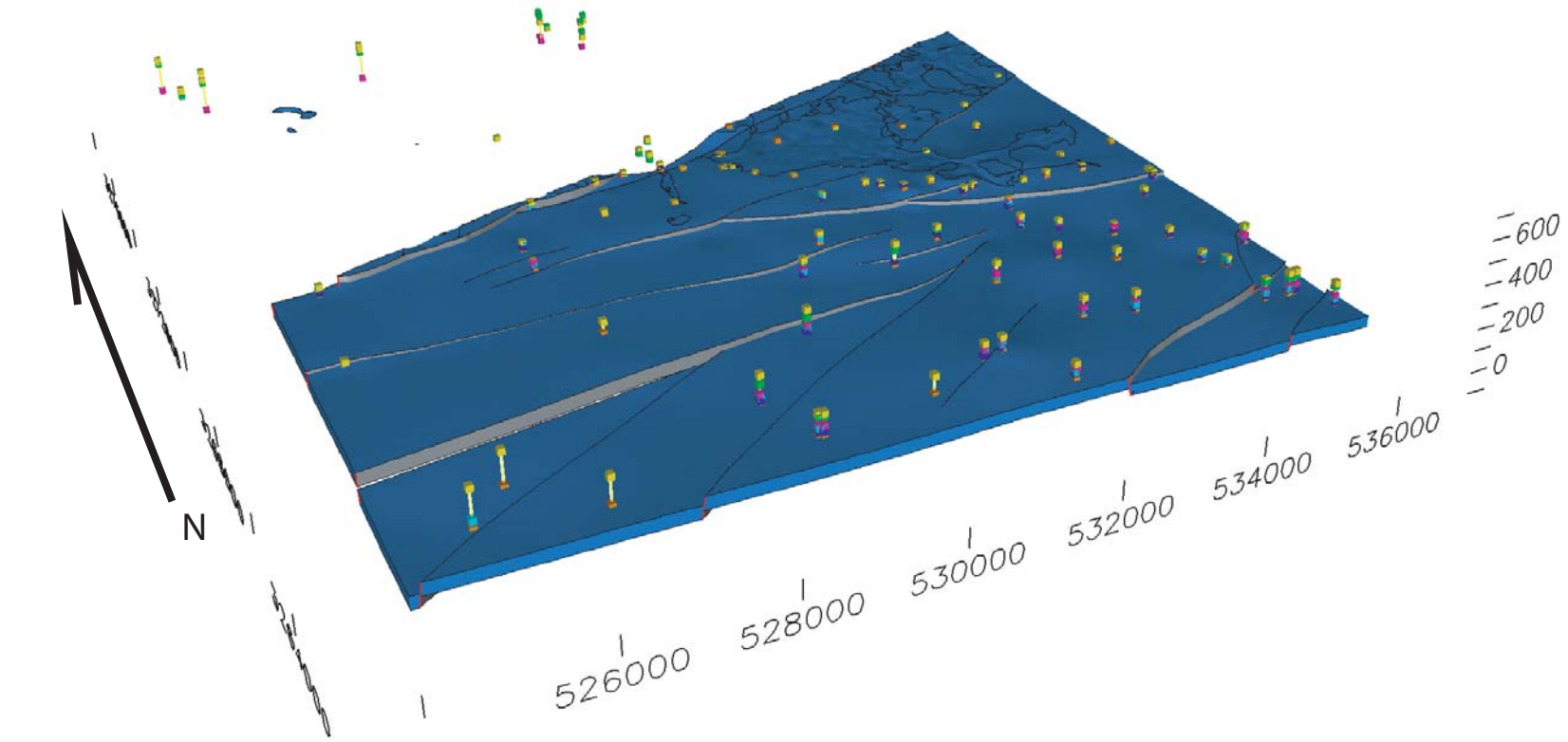

Figure 3-8. Oblique view of the Helotes geologic framework model horizon ‘Georgetown-Person Fms'. Coordinates are UTM meters, NAD27. View direction is NE. Illumination from SW. Yellow points show well locations at land surface, and other points on well bores are stratigraphic picks that can be queried in the geologic framework model.

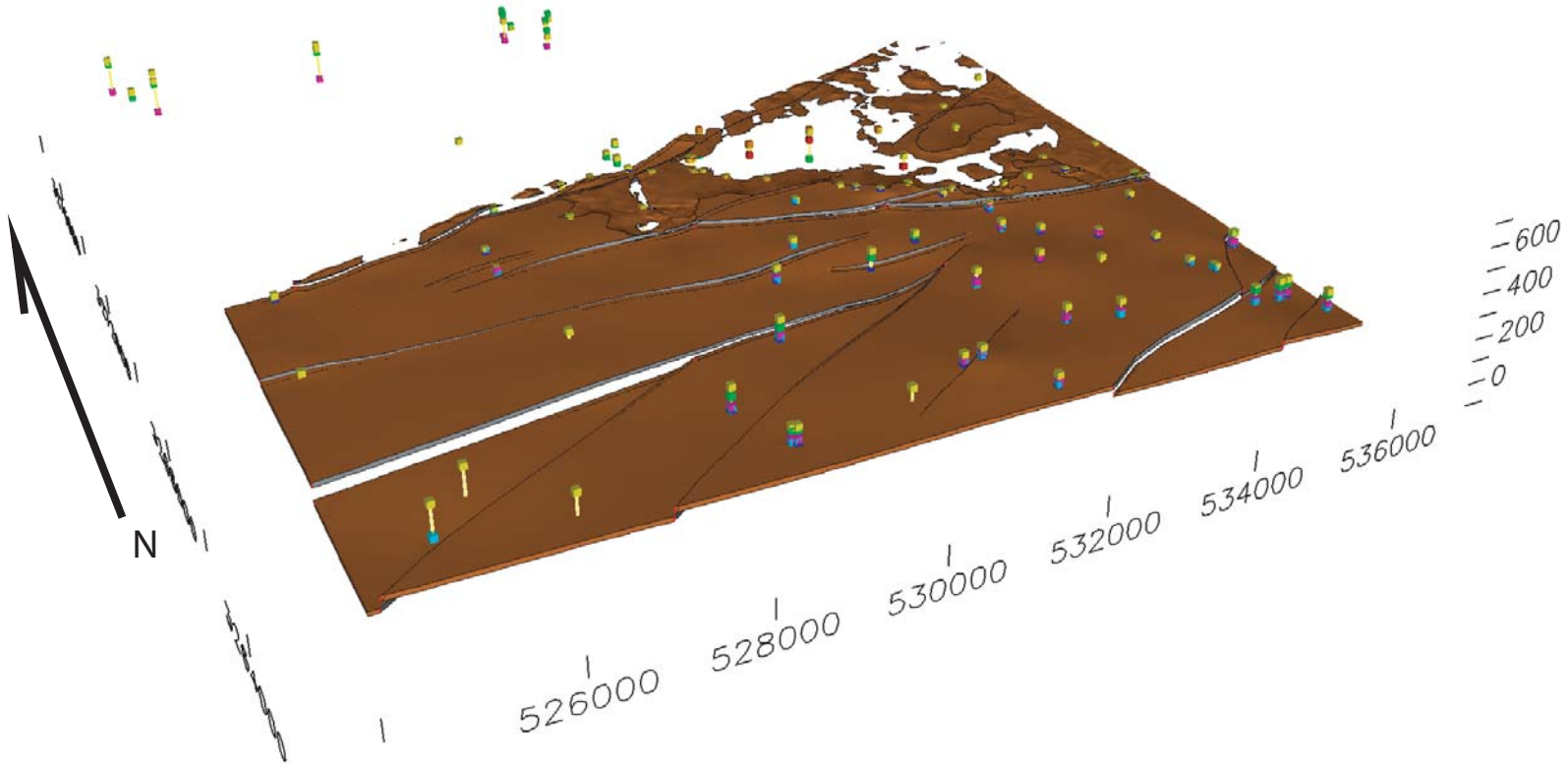

Figure 3-9. Oblique view of the Helotes geologic framework model horizon 'Del Rio Fm'. Coordinates are UTM meters, NAD27. View direction is NE. Illumination from SW. Yellow points show well locations at land surface, and other points on well bores are stratigraphic picks that can be queried in the geologic framework model.

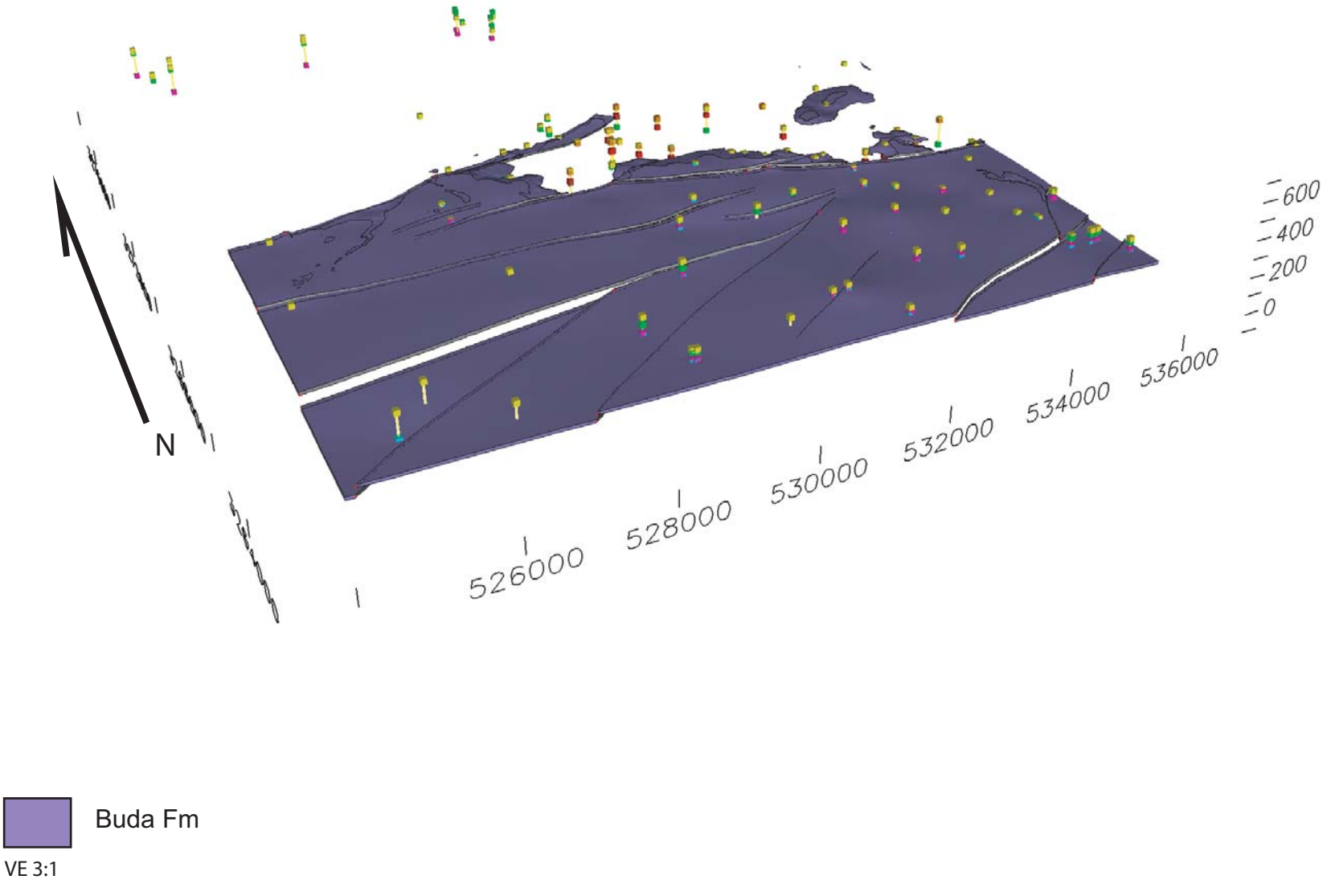

Figure 3-10. Oblique view of the Helotes geologic framework model horizon ‘Buda Fm'. Coordinates are UTM meters, NAD27. View direction is NE. Illumination from SW. Yellow points show well locations at land surface, and other points on well bores are stratigraphic picks that can be queried in the geologic framework model.

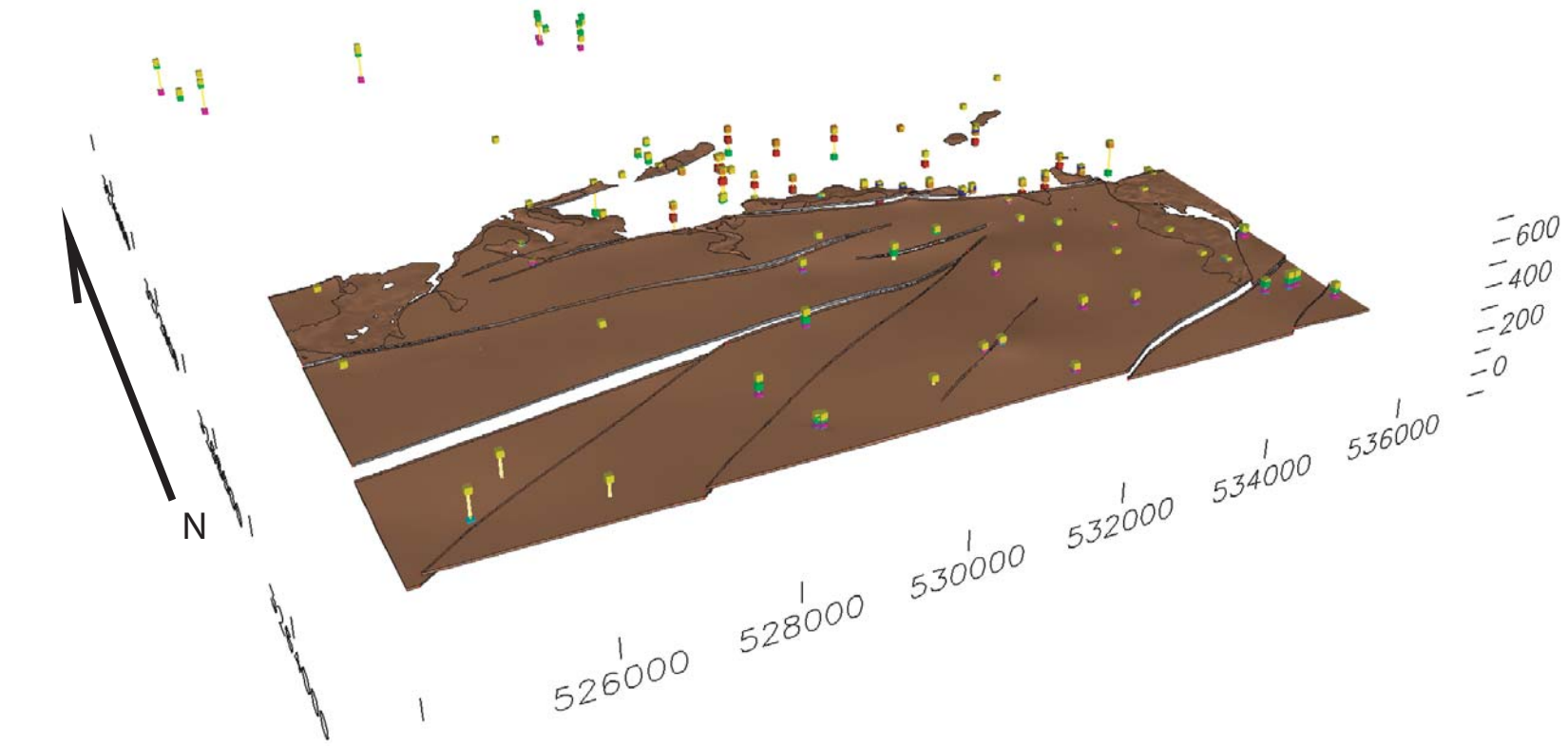

Figure 3-11. Oblique view of the Helotes geologic framework model horizon ‘Eagle Ford Fm'. Coordinates are UTM meters, NAD27. View direction is NE. Illumination from SW. Yellow points show well locations at land surface, and other points on well bores are stratigraphic picks that can be queried in the geologic framework model.

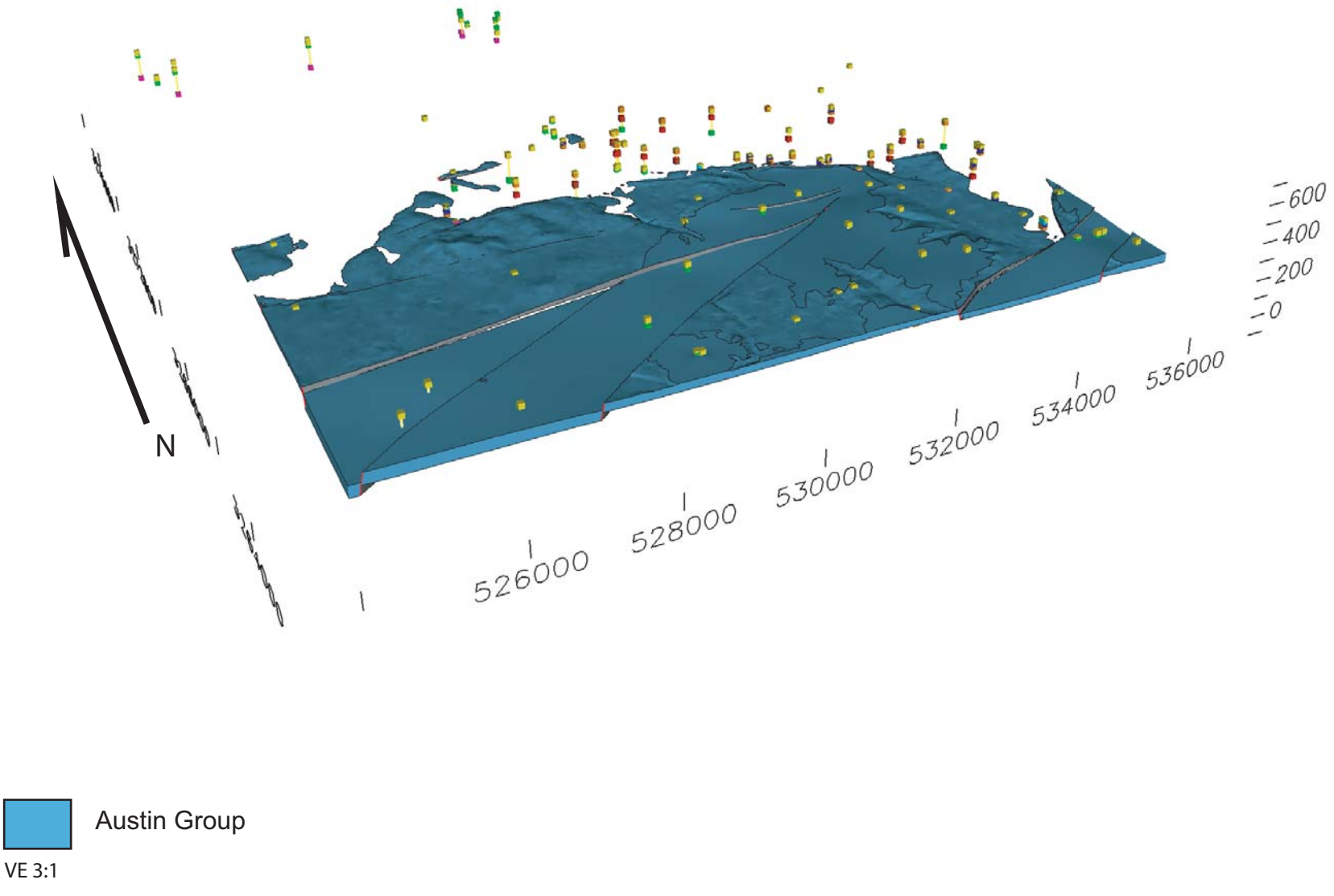

Figure 3-12. Oblique view of the Helotes geologic framework model horizon ‘Austin Gp'. Coordinates are UTM meters, NAD27. View direction is NE. Illumination from SW. Yellow points show well locations at land surface, and other points on well bores are stratigraphic picks that can be queried in the geologic framework model.

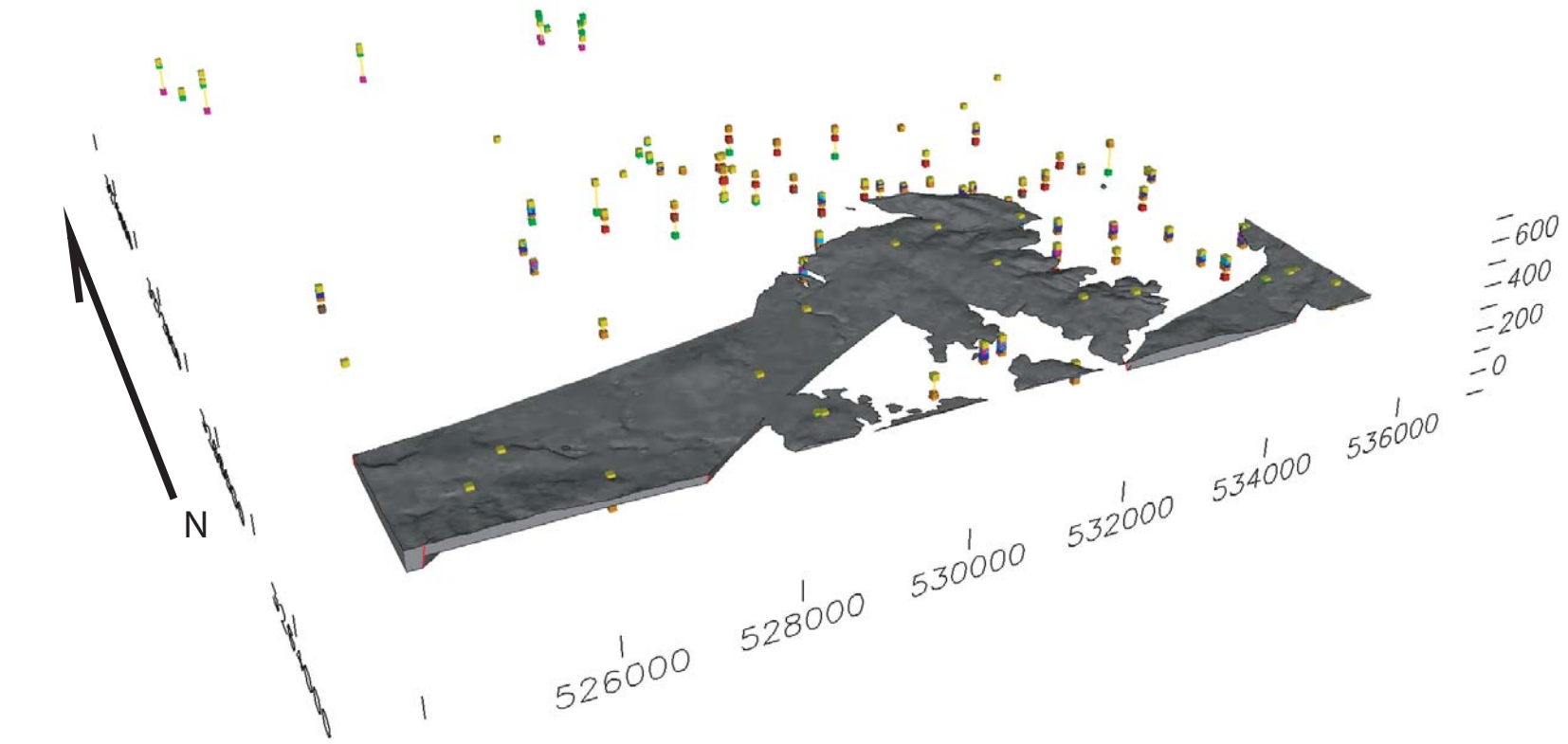

Figure 3-13. Oblique view of the Helotes geologic framework model horizon ‘above Austin Gp'. Coordinates are UTM meters, NAD27. View direction is NE. Illumination from SW. Yellow points show well locations at land surface, and other points on well bores are stratigraphic picks that can be queried in the geologic framework model.

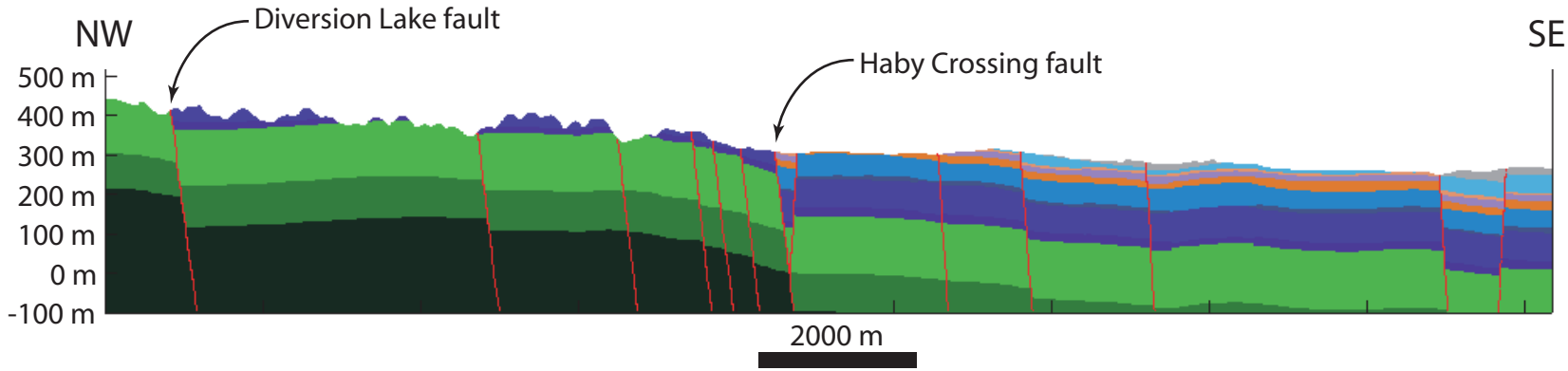

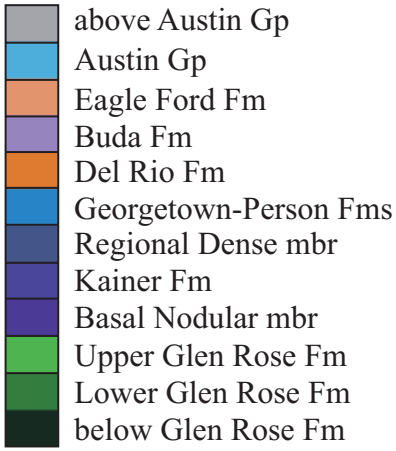

Vertical Exaggeration 5:1

Figure 3-14. Cross section view of the Helotes geologic framework model. Section is oriented NW-SE (see Figure 3-1). Vertical exaggeration = 5:1.

4 FAULT SYSTEM ARCHITECTURE

In the San Antonio region the Balcones Fault System changes trend by 30° from 080° west of San Antonio to 050° northeast of San Antonio. In contrast, individual fault strikes are relatively consistent through the region with an average strike of between 055° and 065° (Figure 4-1; Ferrill et al., 2004). The pattern of faulting in the Balcones Fault System is compatible with having formed in a relatively uniform normal faulting stress field, controlled by vertical maximum principal compressive stress, and horizontal minimum principal compressive stress in the direction 150° (Figure 4-1). Slip tendency is the ratio of resolved shear stress to resolved normal stress on a surface (Morris et al., 1996). At the time of sliding, slip tendency exceeds the frictional resistance to sliding on a fault surface. Slip tendency analysis of the Balcones Fault System indicates that most of the major faults have orientations compatible with southeasterly directed extension (see rose diagram in Figure 4-1; details of analysis are described in Ferrill et al., 2004). Thus the difference between individual fault strikes and the trend of the fault system reflects an *en echelon* fault system. In the early stages of the development of *en echelon* normal fault systems, fault block connectivity tends to remain high, and fault connectivity remains low. With progressive extension, faults link by intersection of curved fault tips or the formation of connecting faults and fault block connectivity declines as fault connectivity increases (Ferrill et al., 1999a; Ferrill and Morris, 2001; Sims et al., 2005).

Northeast and west of San Antonio, a large portion of the displacement associated with the Balcones Fault System is along one primary fault surface or a narrow fault zone associated with the Balcones Escarpment. Through the San Antonio segment, no single fault dominates the displacement of the fault system. Instead, displacement is distributed across a 12 km wide system of faults. Collins and Hovorka (1997) noted that this fault displacement pattern in the San Antonio area represents a stepover between two large-displacement faults, resulting in a broad displacement transfer system or relay ramp (Collins and Hovorka, 1997). The detailed investigation of the Helotes Quadrangle study area is at the western end of this relay ramp. In the vicinity of Helotes, one fault, the Haby Crossing fault, accommodates 30 percent to 50 percent of the total vertical displacement across the Balcones Fault System.

Our analysis uses a combination of field data and results from geologic framework modeling to characterize fault system architecture. The predominant stratigraphic units that crop out in this area are the Glen Rose Formation with isolated outcrops of younger Edwards Group rocks (Collins, 2000). Rocks of the Glen Rose Formation are not well exposed within the study area and, to fully characterize the nature of faulting in this formation, we extended the field analysis to adjacent areas where these lithologies can be studied in surface exposures (Ferrill et al., 2003). These exposures include faults with displacements ranging from <1 m (3 ft) to tens of meters in the Upper and Lower Glen Rose Formations. The most spectacular exposure is in the spillway of Canyon Lake where bedrock of the Upper Glen Rose Formation was exhumed by flooding in July 2002. One fault in the spillway gorge exposure, the Hidden Valley fault, has displacement of approximately 61 m (200 ft) (George, 1952) and is exposed laterally for a distance of >500 m (1640 ft). This fault zone both recharges and discharges groundwater along its exposed length and is an excellent example for detailed investigation of fault zone characteristics and relevance for groundwater movement within the Glen Rose Formation. Several other faults with smaller displacements (<1 m (3 ft)) are exposed for tens of meters along strike in the spillway gorge. In several places these faults have evidence of dissolution and precipitation of calcite associated with the fault zone. At several locations, these small-displacement faults consistently discharge flowing water (also see Section 7).

4.1 Fault Juxtaposition of Stratigraphy

Faulting can juxtapose layers of different permeability characteristics. Displacement gradients on faults can produce complicated juxtaposition relationships so that originally continuous layers are partially or completely separated across faults, and layers that were originally vertically separated from one another can be juxtaposed by fault displacement. This means that with increasing fault displacement, original hydraulic communication pathways are diminished or broken and new pathways may be formed through karst processes. Simple geometric juxtaposition analysis as described by Allan (1989) assumes that the fault zone has no particular properties that cause it to differ from unfaulted host rock. Maclay and Small (1983) and Maclay (1989) used a similar approach to analyze juxtaposition of permeable zones and relatively impermeable zones in the Edwards Aquifer. The geometric effects of faulting of the Edwards and Trinity Aquifers' stratigraphic section are illustrated in Figure 4-2.

Viewing the Upper Glen Rose Formation model layer in 3-dimensions reveals that with one exception, fault displacements within the area of this study are too small to place the base of the Edwards Aquifer (basal nodular layer) against the permeable Lower Glen Rose Formation layer (Figure 4-3). The one notable exception is the Haby Crossing fault. Note that, regardless of displacement, each fault thins the strata that are cut by the fault, causing thinning of both aquifer and aquitard layers. Structural thinning of aquifer layers can cause flow constrictions, and areas of such flow constrictions can be identified using a map of fault throw (vertical component of fault displacement) distribution as described in the next section. Nevertheless, karst dissolution features may develop that follow or cross faults that appear to be barriers based on geometrical (thinning and juxtaposition) relationships alone, enhancing inter-aquifer communication (also see Sections 5 and 7).

4.2 Fault Throw Distribution

The vertical component of displacement (throw) on faults in the Helotes study area was measured using the fault gaps at the top of the Edwards Aquifer reference horizon (top of Georgetown Formation). Throw values range from 0 m at fault tips to a maximum of approximately 178 m (584 ft) (Figure 4-4).

In the Helotes Quadrangle area the Haby Crossing fault accommodates more than 100 m (328 ft) of throw along its entire length. This is sufficient to juxtapose most of the thickness of the lower, more transmissive (Maclay, 1989) Kainer Formation (including the Basal Nodular member) with the Upper Glen Rose Formation (Figure 4-5).

4.3 3DStress™ Analysis

Slip tendency analysis (e.g., Morris et al., 1996; Ferrill et al., 1999b) of the Helotes Quadrangle fault system is based upon two principal assumptions and field observations of faults exposed in the Glen Rose Formation in the vicinity of the study area. First, we assume the rocks of the Glen Rose Formation were deformed during the middle to late Tertiary (Murray, 1961; Young, 1972) beneath an overburden that included the younger Cretaceous rocks of the region and the lower to middle Tertiary formations. The total overburden thickness was likely of the order of 0.9 km (0.6 mile) (e.g., Collins, 2000). Second, the rock column above the Glen Rose Formation was essentially water-saturated at the time of deformation. Approximate magnitudes of the principal stresses can be obtained from these assumptions. Normal faults predominate those observed in the field in this study and by other workers throughout the Balcones Fault zone, therefore the vertical stress at the time of faulting would have been the maximum principal effective stress (σ_1'). Using the assumptions of overburden thickness and rock column saturation (above), σ_1'would have been equal to the lithostatic stress (here based on an average rock density of 2.7 gm/cm^3)

minus the hydrostatic pore water pressure, yielding a vertical effective stress of 15 MPa. For faulting to have occurred, the differential stress must have been sufficient to generate a maximum slip tendency of about 0.7 (Morris et al., 1996). We estimate the minimum horizontal effective stress (σ_3') to have been 4 MPa. Field observations of slickenlines indicate that rakes of slip vectors were steep (Ferrill et al. 2003, 2004). In other words, faults of almost all strikes experienced near dip-slip displacement. To accomplish this, we chose a σ_2' value of 9.5 MPa. Azimuths of the two principal horizontal stresses were established by visually fitting the slip tendency data to poles of measured fault surfaces (Ferrill et al., 2003; 2004) in the Glen Rose Formation in and around the study area. This analysis yielded an extension azimuth of 150°.

Applying this inferred stress system (using 3DStress v. 3.0; Southwest Research Institute, 2003) to the fault surfaces exported from the three-dimensional model (Figure 4-6) indicates that the large, east northeast–west southwest striking faults were favorably oriented to have accommodated regional strains by normal fault movement. The fault system within the Helotes study area is dominated by faults that are consistent with the regional trend of the Balcones Fault zone, and these faults probably formed in response to the stress tensor inferred from the 3DStress™ analysis. Faults with 75° dips experience lower values of slip tendency (Figure 4-6a), but nevertheless represent the fault orientation most likely to have developed within the more competent and less deeply buried Edwards Aquifer rocks (Ferrill and Morris, 2003). Faults with northwest to southeast strikes are not mapped at the scale of resolution of the three-dimensional model, indicating that local perturbations resulting from such effects as displacement-gradient-driven fault block deformation were not widely developed in this area, or generated only small-displacement faults. In addition to experiencing high slip tendencies in the inferred stress system, the predominant faults, especially those with steep dips, are also subject to high dilation tendencies (Figures 4-6b; Ferrill et al., 1999b). Dilation tendency is the likelihood that a fracture or fault will be open (dilate) and thus be more transmissive to fluid flow. This combination of high slip and dilation tendencies implies that the major faults would have been effective fluid transmission pathways, subject to the constraints of fault zone architecture, at the time of faulting (Finkbeiner et al., 1997; Ferrill et al., 1999b). If a similar stress system were extant today, the faults would be in favorable orientations for fluid transmission.

North of the Haby Crossing fault, and in a narrow (less than 500 m, 1640 ft, wide) band just south of it, faults are closely aligned with the optimal strike for the inferred regional stress system. South of the Haby Crossing fault, there is more variability. Eight faults are parallel to the main trend (including all the down-to-the-north faults), but the remaining six faults have more east-west or even east-southeast to west-northwest strikes. This part of the Helotes area lies at the western end of the San Antonio relay ramp (Collins, 1993) and these latter faults may be the result of rotated stresses within that ramp (Ferrill and Morris, 2001).

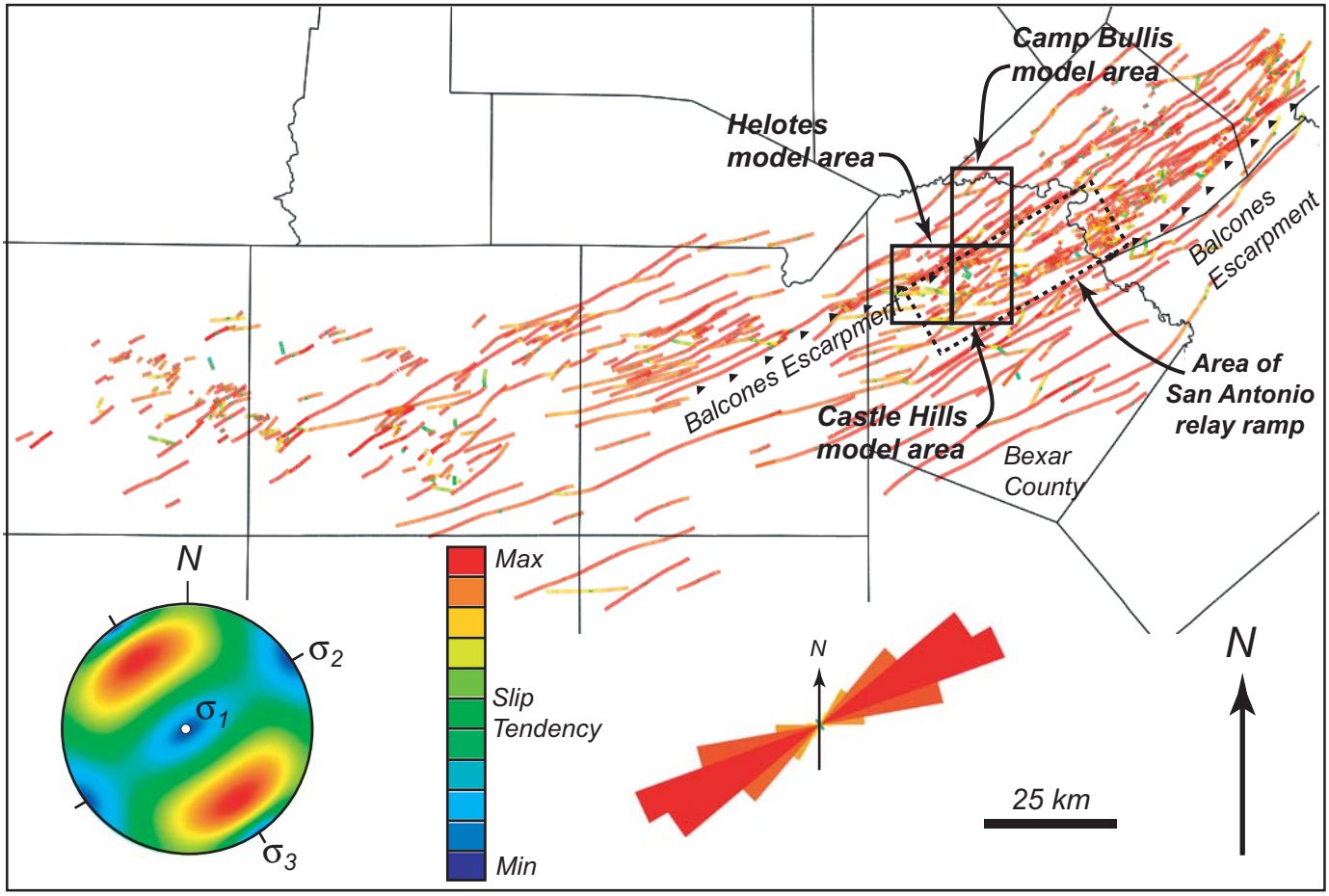

Figure 4-1. Map of the Balcones fault system in the San Antonio area with fault traces colored according to their slip tendencies. Slip tendency analysis was performed using 3DStress™ v. 1.3.3 (see Ferrill et al., 2004) based on mapped faults of Collins and Hovorka (1997).

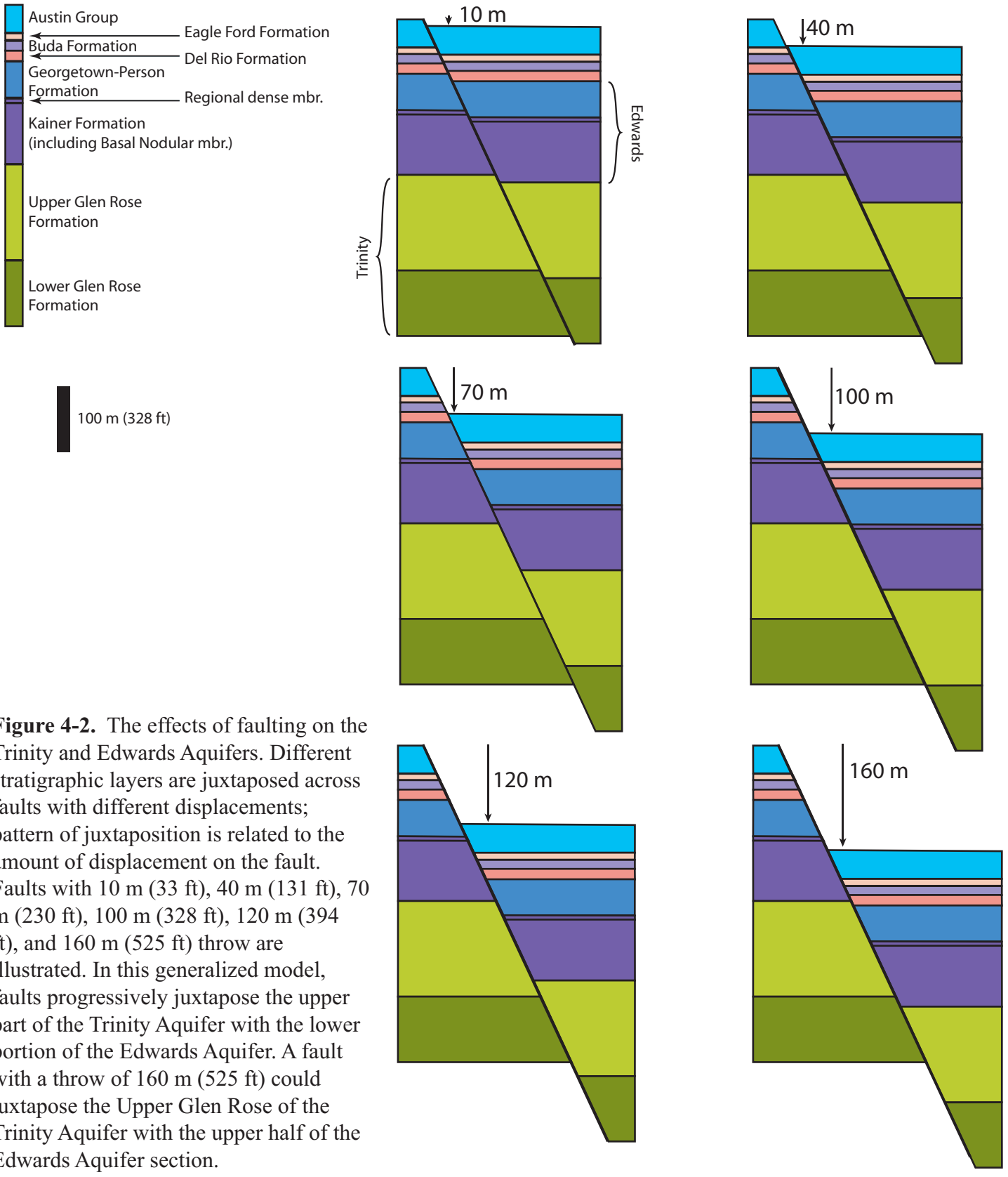

Figure 4-2. The effects of faulting on the Trinity and Edwards Aquifers. Different stratigraphic layers are juxtaposed across faults with different displacements; pattern of juxtaposition is related to the amount of displacement on the fault. Faults with 10 m (33 ft), 40 m (131 ft), 70 m (230 ft), 100 m (328 ft), 120 m (394 ft), and 160 m (525 ft) throw are illustrated. In this generalized model, faults progressively juxtapose the upper part of the Trinity Aquifer with the lower portion of the Edwards Aquifer. A fault with a throw of 160 m (525 ft) could juxtapose the Upper Glen Rose of the Trinity Aquifer with the upper half of the Edwards Aquifer section.

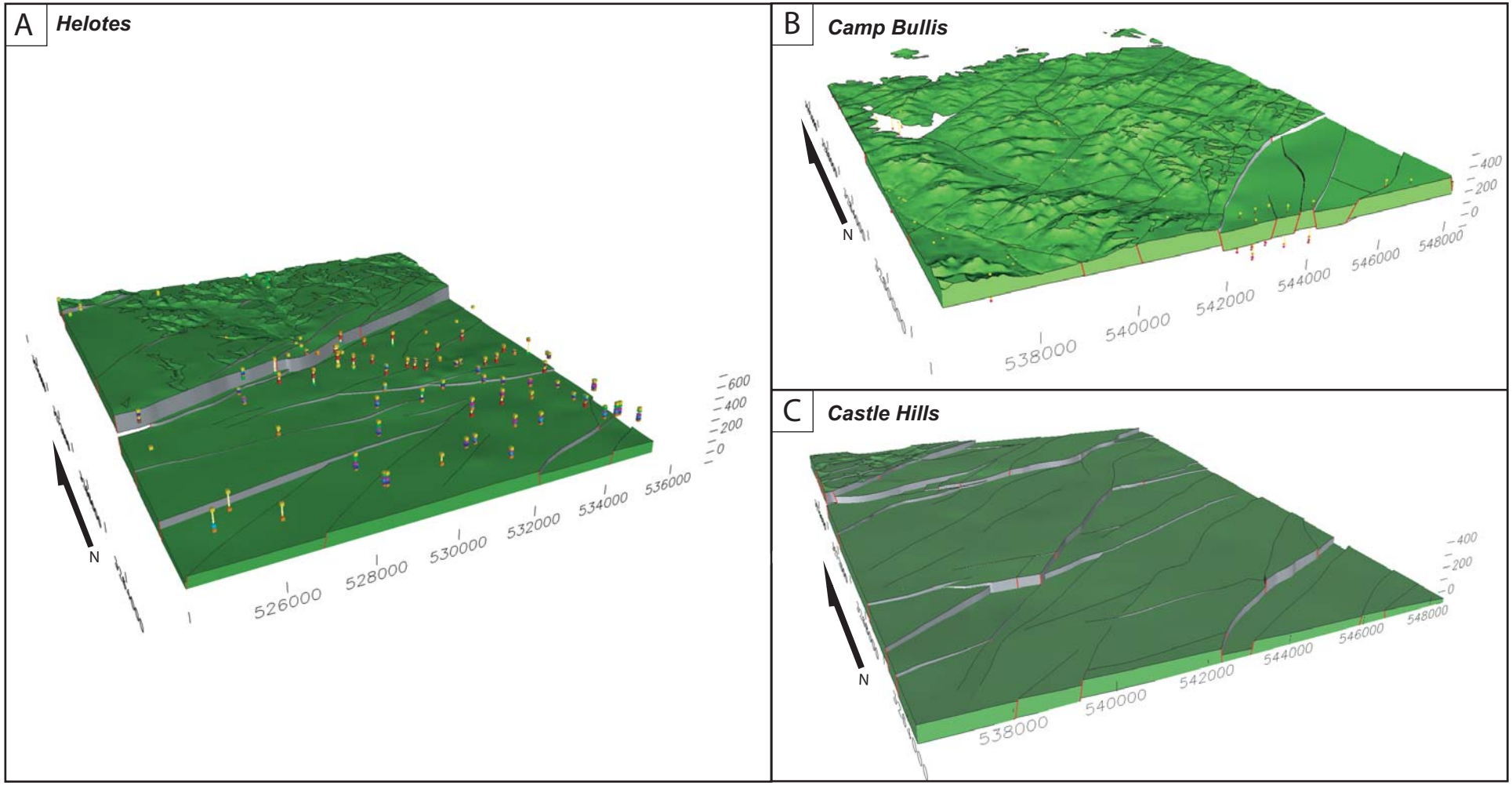

Figure 4-3. Oblique views of Upper Glen Rose Fm. model layer in the (A) Helotes geologic framework model, (B) Camp Bullis geologic framework model, and (C) Castle Hills geologic framework model.

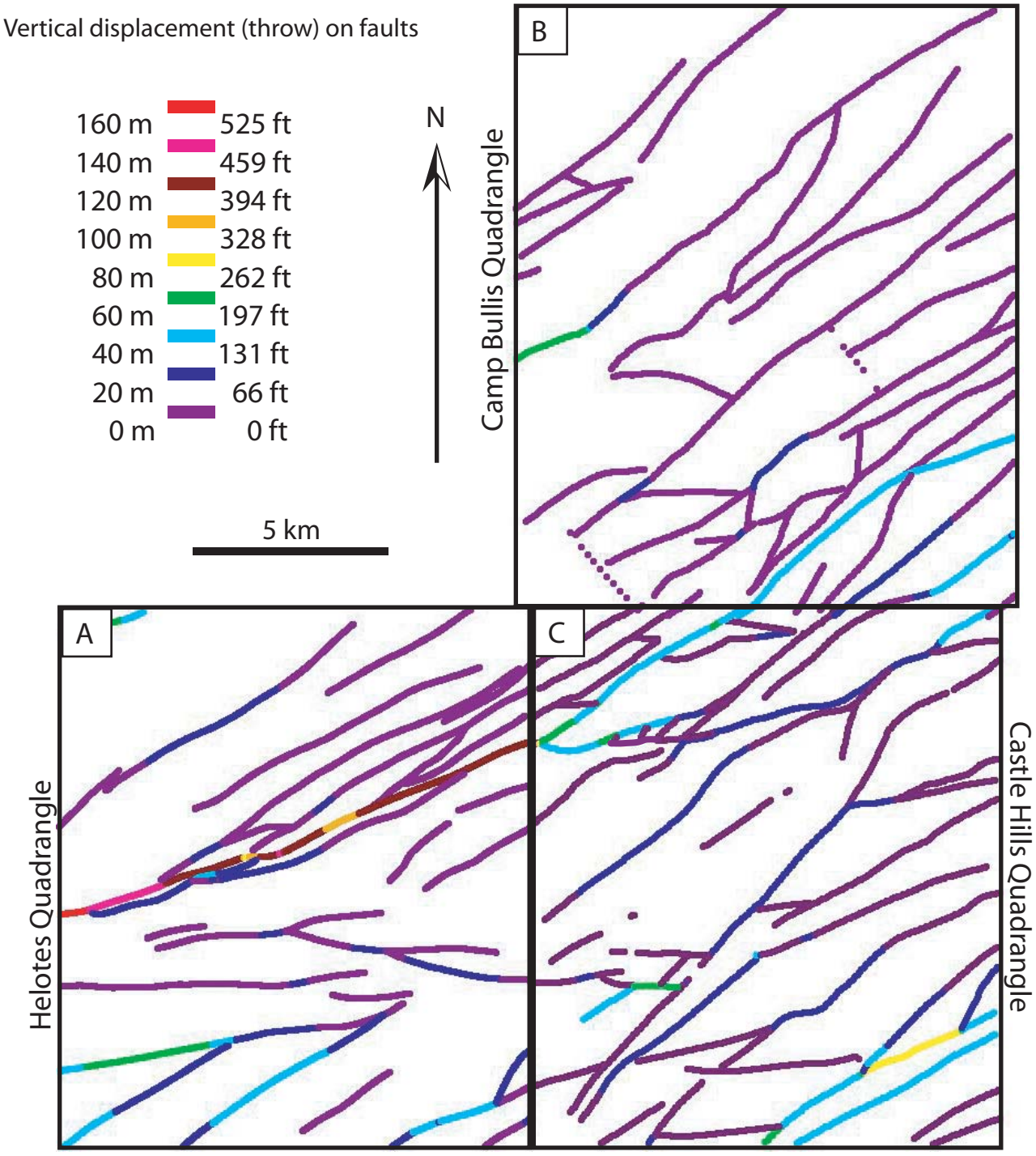

Figure 4-4. Throw map at the top of the Edwards Aquifer (Georgetown Fm.) in the Helotes study area, combined with the throw map at the top of the Lower Glen Rose Fm. in the Camp Bullis area (Ferrill et al., 2003) and the Upper Glen Rose Fm. in the Castle Hills quadrangle (after Ferrill et al., 2004).

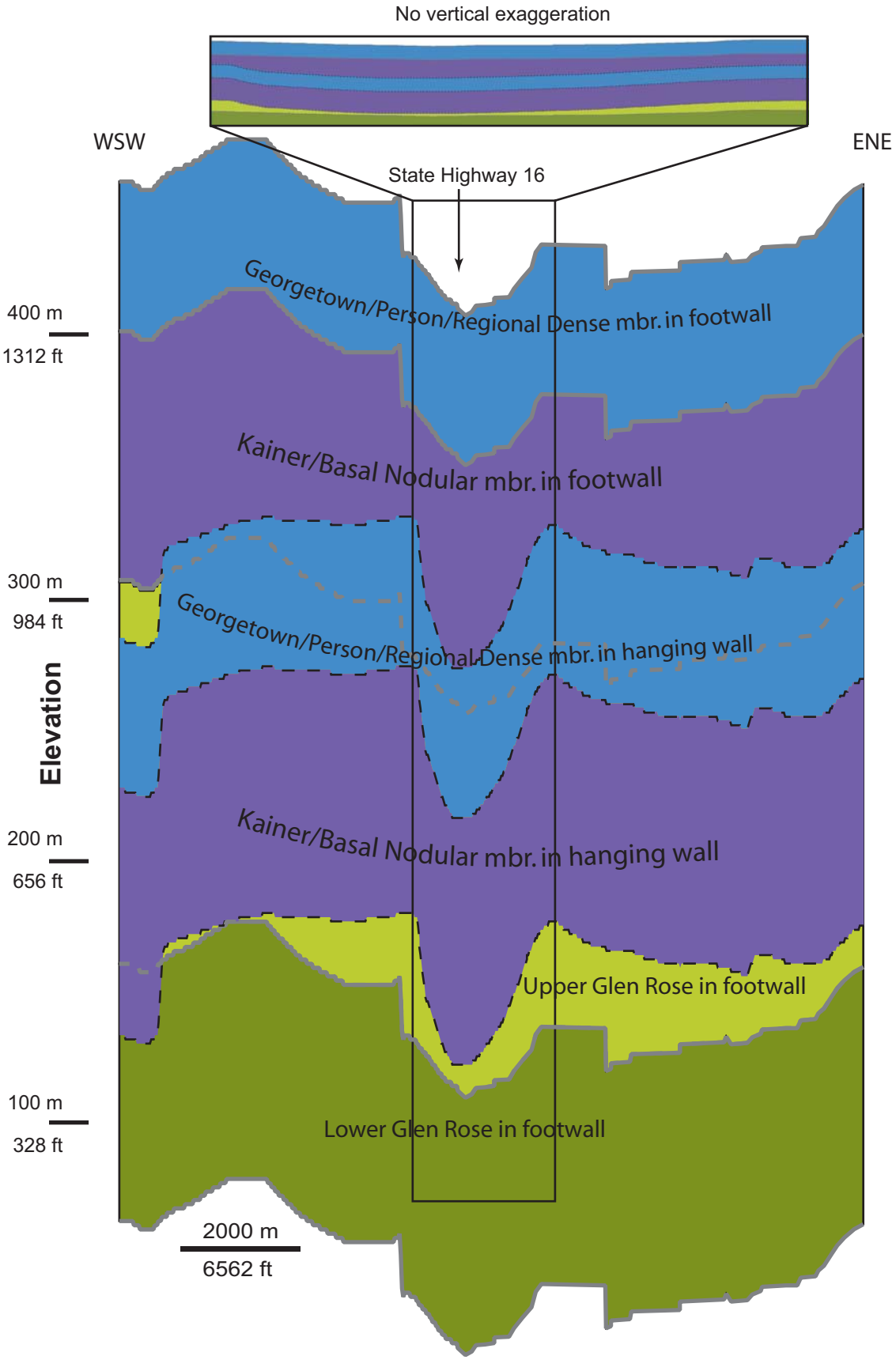

Figure 4-5. Allan diagram for the Haby Crossing fault. Hanging wall stratigraphy (two principal divisions of the Edwards only) is outlined in dashed black lines; footwall stratigraphy outlined in gray solid and dashed lines.

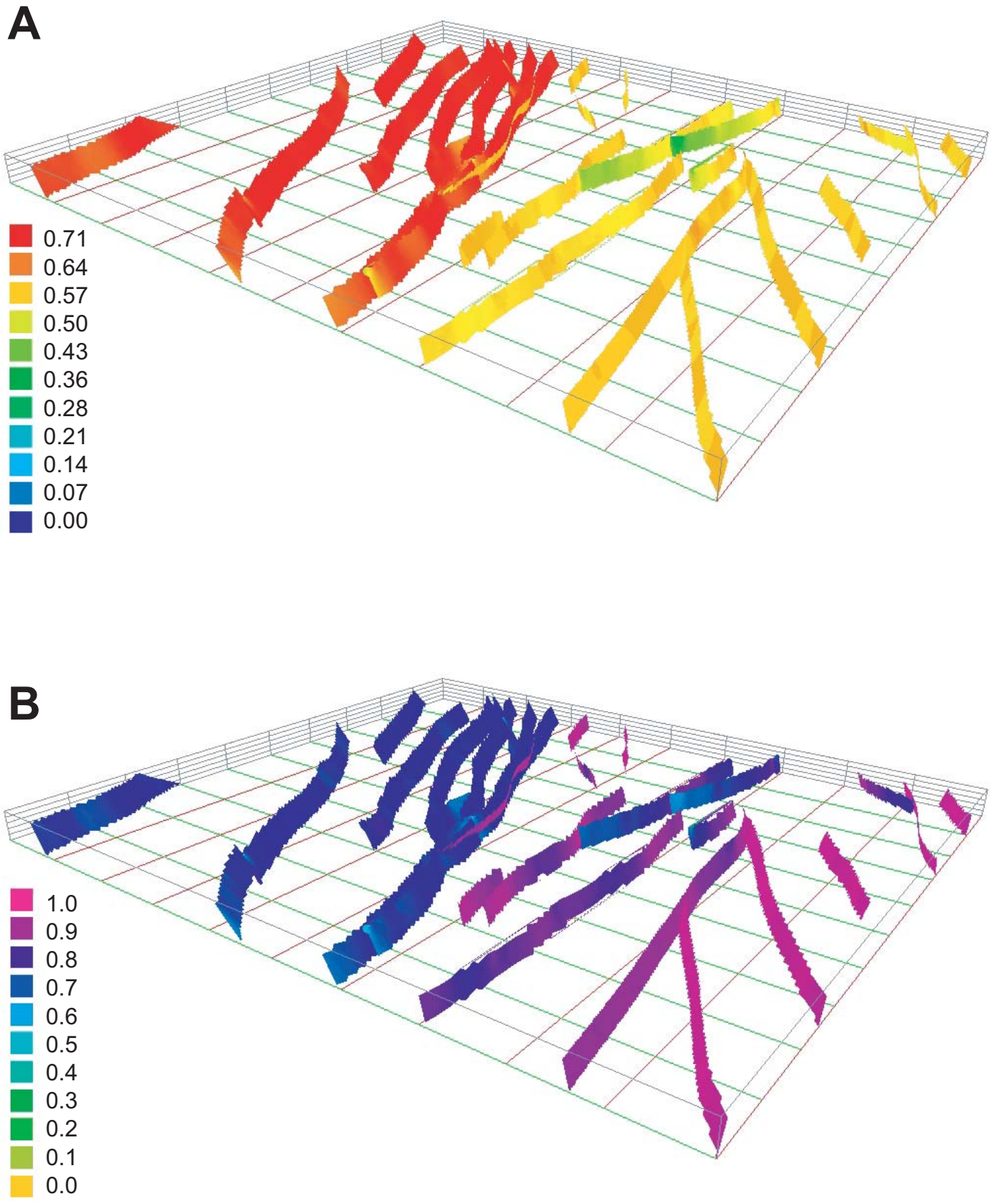

Figure 4-6. Three-dimensional fault surfaces from geologic framework model color coded according to (A) slip tendency and (B) dilation tendency (σ_1 = 15 MPa, vertical; σ_2 = 9.5 MPa, 060°; σ_3 = 4 MPa, 150°).

5 FAULT ZONE DEFORMATION

5.1 Introduction

In this section, we present the results of fault zone deformation investigations conducted in the Cretaceous limestone and shale section, with emphasis on investigations of the Glen Rose Limestone, and comparisons with fault zone deformation in the Edwards limestone (Ferrill and Morris, 2003; Ferrill et al., 2004). The overall *en echelon* geometry of the Balcones Fault system would, in general, be expected to produce poorly connected faults and result in well connected layers early in fault system development. Competing with this development is the apparent rapid lateral propagation of fault segments with increasing displacement, at least within stronger mechanical layers (Ferrill et al., 2004). This rapid propagation is expected to result in relatively early interconnection of faults and loss of stratigraphic communication pathways due to development of through-going faults. Field observations show that vertical connectivity is tied to mechanical stratigraphy and that weak mechanical layers at the formation to member scale are capable of arresting fault tip propagation (Ferrill et al., 2003).

Fault zone deformation involves mechanical and chemical alteration of rock properties, both in the principal displacement zone (fault core) and the zone of less intense fault damage (damage zone), developed adjacent to the fault core (Caine et al., 1996). The Glen Rose Formation consists of limestones and shales, and the Upper Glen Rose Formation in particular is composed of alternating well-bedded limestones and shales. This lithological character leads to lower mechanical competence compared with the overlying Edwards limestones and, coupled with the greater depth of burial during faulting, results in gentler fault dips and a different faulting character than in the Edwards limestones.
Deformation within fault zones results in faults serving as barriers to flow, pathways for flow, or both. Fault zone deformation is by definition localized along faults, and its distribution is therefore controlled by the architecture of the fault systems. The mechanisms of deformation within fault zones depend on the host lithologies, fault system architecture (e.g., Ferrill et al., 2003), and deformational environment (e.g., Ferrill and Morris, 2003).

Although lateral displacement gradients appear to be relatively gentle throughout the Balcones Fault zone (Ferrill et al., 2004), there may be local anomalies, such as on the Haby Crossing fault, and there is evidence that vertical displacement gradients are locally pronounced and controlled by stratigraphy. Stratigraphic control is to be expected where strongly contrasting mechanical layers are faulted. Normal faulting in single, mechanically strong layers has been the subject of intensive investigation by numerous workers over the past decade. These analyses have shown that folding prior to or during fault propagation along faults tends to be limited, and most commonly occurs between laterally or vertically overlapping fault tips (Grimshaw and Woodruff, 1986; Larsen, 1988; Peacock and Sanderson, 1994; Trudgill and Cartwright, 1994; Huggins et al., 1995; Childs et al., 1996; Ferrill et al., 1999a). A mechanically weak layer within the deforming stratigraphic section can serve as a décollement and result in disharmonic deformation. The presence of a weak décollement layer may result in significant monoclinal folding prior to fault breakthrough (Withjack et al., 1990). Thus, the most likely locations for fault tip monoclines to form is where faults in a strong mechanical layer intersect a weak mechanical layer. The style of deformation and structural disharmony depends on the effective mechanical contrast between the deforming layers under the conditions of deformation, and thicknesses of the contrasting units. Monoclines commonly develop structurally above faults that terminate below the ground surface and where the rate of fault propagation is relatively slow with respect to the rate of fault displacement. Consequently, folding occurs above and laterally beyond fault tip lines. Depending on the location of

breakthrough, this process will leave synthetic dip panels (rock dipping in the same direction as the fault) in either the hanging wall or footwall, or both.

5.2 A Model for the Evolution of Large-Displacement Faults in the Glen Rose Formation, Edwards Group, Del Rio Formation, and Buda Formation

5.2.1 Faults with throws of 10 m (33 ft) or less

In limestones of the Edwards Aquifer (primarily the Person and Kainer Formations) small-displacement faults typically dip at 70° to 75° and are represented by narrow (1 to 5 cm, 0.4 to 2 inches) fault zones. Numerous faults with displacements ranging from 0.5 cm to 1 m (0.2 inches to 3 ft) develop in the footwall and hanging wall adjacent to such faults. Variation in bed dip associated with these faults is minimal (Figure 5-1a). Fault zones may contain cataclasite derived from the wall rock, dissolution may create permeability along portions of the fault, and thin shale layers may be discontinuously smeared onto the fault surface (Figures 5-1a and 5-2). The response of the overlying Del Rio, Buda, Eagle Ford, and Austin Formations is markedly different. The shale-rich Del Rio Formation commonly arrests fault propagation for displacements of 10 meters (33 ft) or less, and deforms in a ductile manner. Above the Del Rio Formation, monoclinal folding accommodates the displacement even in the more limestone rich Buda and Austin Formations (Figure 5-1b). This creates potential for clay smear on subjacent fault surfaces, and faults with approximately 10 m (33 ft) to as much as 20 m (66 ft) of throw are not likely to juxtapose Buda limestones directly with Edwards rocks (Ferrill et al., 2004; Figure 5-3a). Glen Rose Formation rocks, beneath the Edwards, exhibit a combination of these two styles. Fault dips are typically around 60°, reflecting the greater overburden pressure on these rocks during deformation and their generally higher clay content than Edwards rocks (both pervasively, and as numerous shale interlayers). Well-bedded limestones develop faults, whereas more shaley layers tend to deform in a more ductile fashion. Faults with displacements of around 10 m (33 ft) in limestone layers may be arrested and the displacement accommodated by monoclinal folding in the shale-rich layers (Figure 5-1c, 5-3a). Arrays of small displacement (less than or equal to 1 m or 3 ft), conjugate faults tend to be associated with larger faults (Figure 5-1c), and shaley layers are commonly deformed around these faults without displacement. Small-displacement faults in the limestone layers commonly exhibit slickolites (Figure 5-2c) which attest to the water-saturated condition of the faults during deformation, and continuous dissolution and re-precipitation during fault slip. Dipping panels that probably result from fault propagation both vertically and horizontally are common (Figure 5-4). Fault zones, therefore, tend to be complicated with both permeability enhancement resulting from increased fault frequencies and occlusion of fault zones where shales have been smeared into the fault.

5.2.2 Faults with throws of 50 m (164 ft) to 200 m (656 ft)

The effects of the change in fault dip that occurs at the base of the Edwards Aquifer limestones and the top of the Glen Rose Formation (from about 75° to about 60°) are likely to become more apparent on faults within this range of displacement. Kinematic analysis assuming constant thickness for the hanging wall of a fault with this geometry (Morris and Ferrill, 1999) predicts that a panel dipping at 20° toward the principal fault should develop and widen as displacement on the fault accumulates. However, the nature of the Edwards limestones, and the conditions during deformation, are such that a migrating fold hinge of this type is not likely to have formed. Instead, a series of small-displacement, antithetically dipping faults and monoclines arranged in a synthetically dipping zone would have developed to accommodate the slip of the hanging wall over the bend in the principal fault (Figure 5-3b, c). This would be manifest as a series of narrow graben in the hanging wall, adjacent to the principal fault. These graben

would be most noticeable adjacent to the largest displacement faults such as the Haby Crossing Fault (Figure 5-3d). Faults in this displacement range will have completely breached the shaley horizons of the Del Rio, Eagle Ford, and Glen Rose Formations. Fault zones in the Edwards consist of cataclasite, calcite cement and dissolution cavities. In the Glen Rose Formation, fault zones are thicker (up to 5 m, 16 ft, thick) and comprise a complex of detached and partially detached relay ramps, zones of highly faulted and fractured limestone, and variable patches of clay smear with dissolution cavities.

5.3 Fault Zone Permeability

In general, faults within the Edwards limestones will be more dilatant than those in the Glen Rose Formation, primarily because of their steeper dips and the more competent lithologies in the Edwards (Ferrill and Morris, 2003). With the exception of clay or shale smear, most fault zone deformation increases permeability within and near faults in all stratigraphic horizons. This is born out by the common occurrence of dissolution features associated with faults (Figure 5-1a; Ferrill et al., 2003) and the importance of faults as recharge features (Clark, 2000). However, fault zone permeability is highly heterogeneous and affects flow both parallel and perpendicular to the fault zone. Although cataclasis and dilation are common in faults cutting Edwards limestones, secondary calcite is also common (Figure 5-2). The timing of this calcite formation is crucial to the development of fault zone permeability. Early cementation, or cementation concurrent with fault slip, will effectively seal the fault. A fault zone consisting of discontinuous patches of cemented fault rock and clay smear will likely permit fault-parallel flow, but across-fault flow will be inhibited unless dissolution passages form.

Faults within the Glen Rose Formation are extremely complex: fault zones and their associated damage halo tend to be wide, bed dips are complex, and clay or shale smear are common (Figures 5-1c, 5-3c, and 5-4). Field observations at the Canyon Lake spillway gorge indicate that fault zone permeability is linked in part to the adjacent stratigraphy. Where significant (1 to 3 m, 3 to 10 ft, thick) shale horizons are present the fault zone will likely seal, and where detached or partially detached relay ramps of limestone are present, these may act as conduits for flow. Surface water is observed to (i) flow in the fault zone, (ii) recharge into, and (iii) discharge from the Hidden Valley fault in the Canyon Lake spillway gorge, attesting to their complex hydrologic behavior and the importance of such faults as flow pathways.

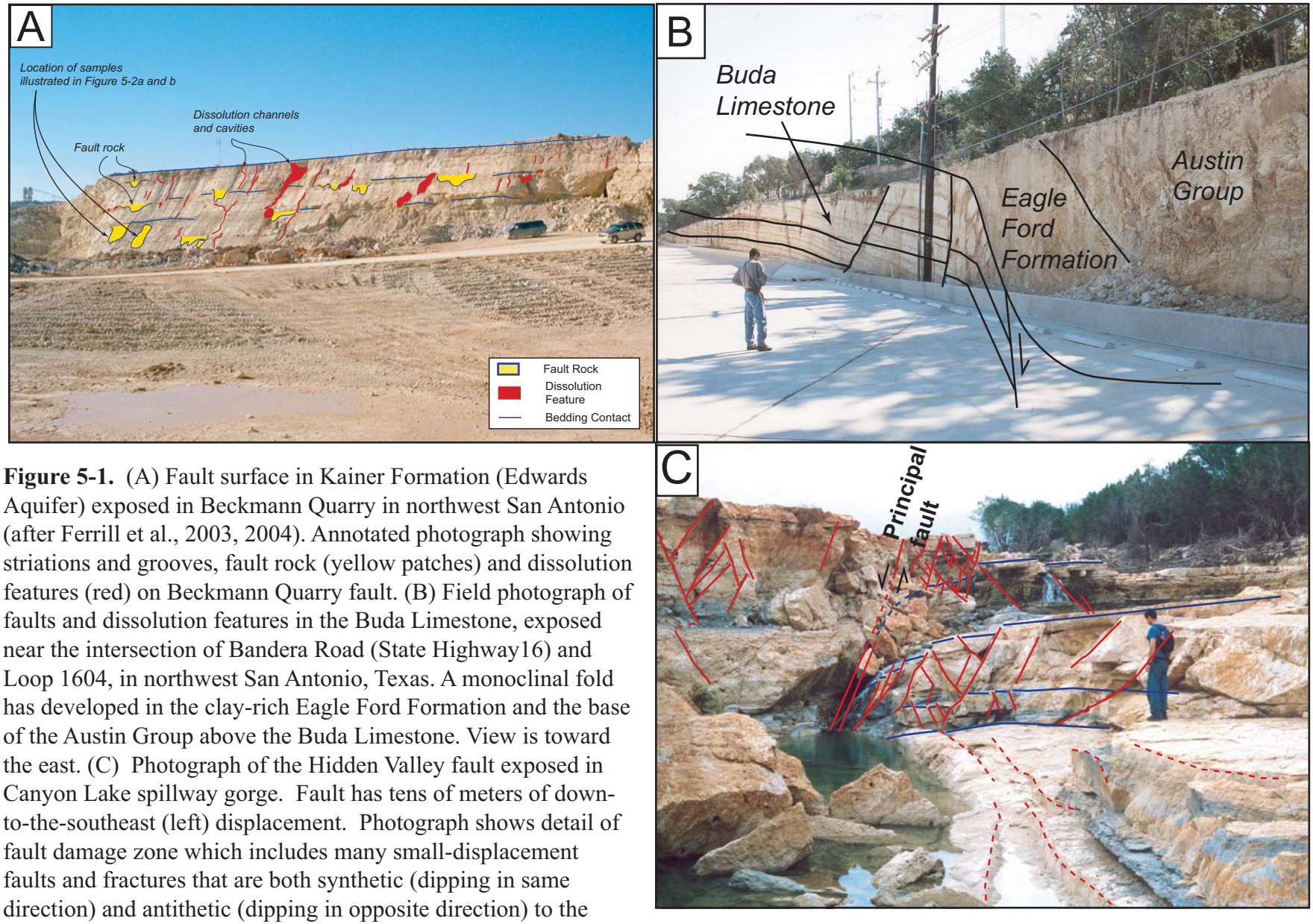

Figure 5-1. (A) Fault surface in Kainer Formation (Edwards Aquifer) exposed in Beckmann Quarry in northwest San Antonio (after Ferrill et al., 2003, 2004). Annotated photograph showing striations and grooves, fault rock (yellow patches) and dissolution features (red) on Beckmann Quarry fault. (B) Field photograph of faults and dissolution features in the Buda Limestone, exposed near the intersection of Bandera Road (State Highway16) and Loop 1604, in northwest San Antonio, Texas. A monoclinal fold has developed in the clay-rich Eagle Ford Formation and the base of the Austin Group above the Buda Limestone. View is toward the east. (C) Photograph of the Hidden Valley fault exposed in Canyon Lake spillway gorge. Fault has tens of meters of down-to-the-southeast (left) displacement. Photograph shows detail of fault damage zone which includes many small-displacement faults and fractures that are both synthetic (dipping in same direction) and antithetic (dipping in opposite direction) to the main fault. Conjugate faulting of this style is expected to produce anisotropic permeability as discussed by Ferrill et al. (1999b; 2000). Synthetic dip is present in the footwall of the main displacement fault core and layer attenuation and shale smear are also visible. Many of the faults exhibit cross-cutting, conjugate relationships (Ferrill et al., 2000).

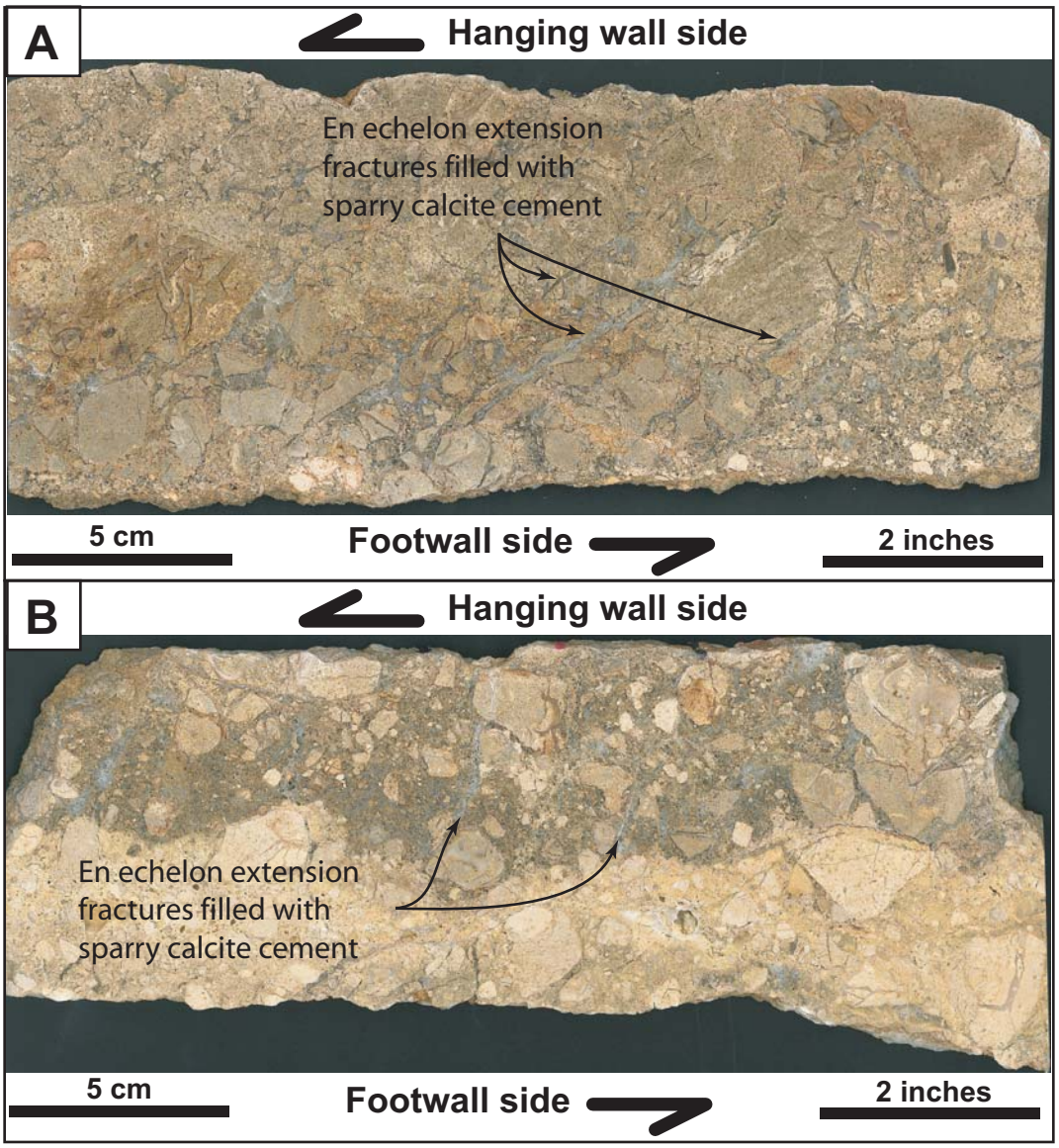

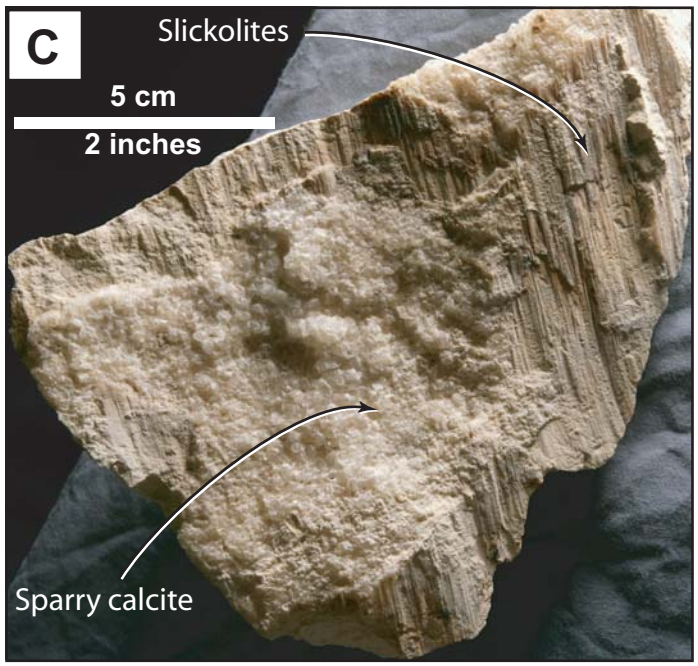

Figure 5-2. Hand sample photographs of fault rocks. (A) and (B) Cataclasite consisting of a wide range of grain sizes. Grains are cemented by sparry calcite, and cut by en echelon extension fractures filled with sparry calcite cement. Samples from Edwards limestone in Beckmann Quarry (see Figure 5-1a). (C) Slickolite lineations formed by simultaneous slip and pressure solution along fault surface. Sparry calcite precipitated in dilational jogs on fault surface. Sample from Upper Glen Rose Formation.

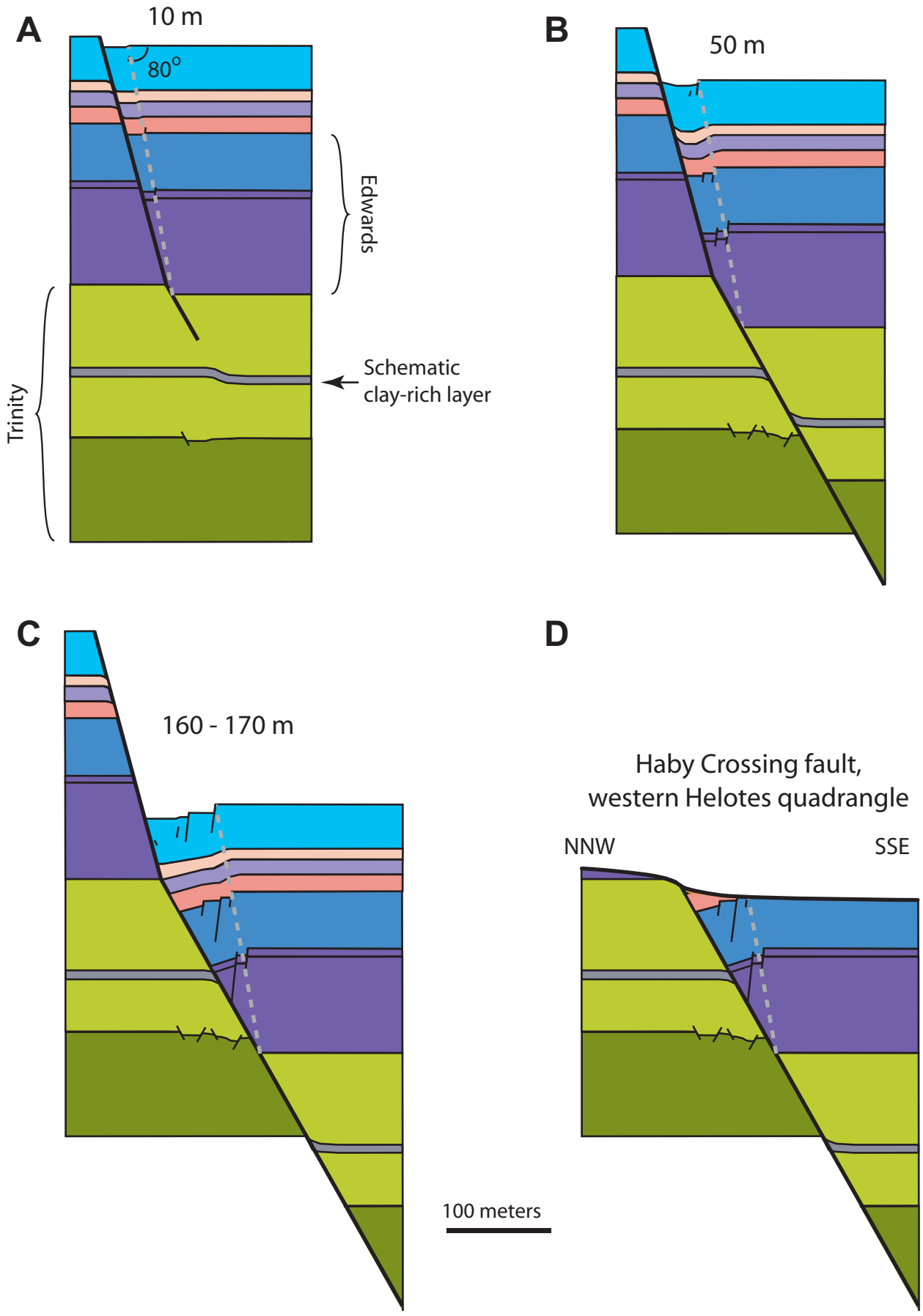

Figure 5-3. Development of a large-displacement fault cutting both Edwards and Trinity Aquifers. Colors as for Figure 4-2. See text for explanation.

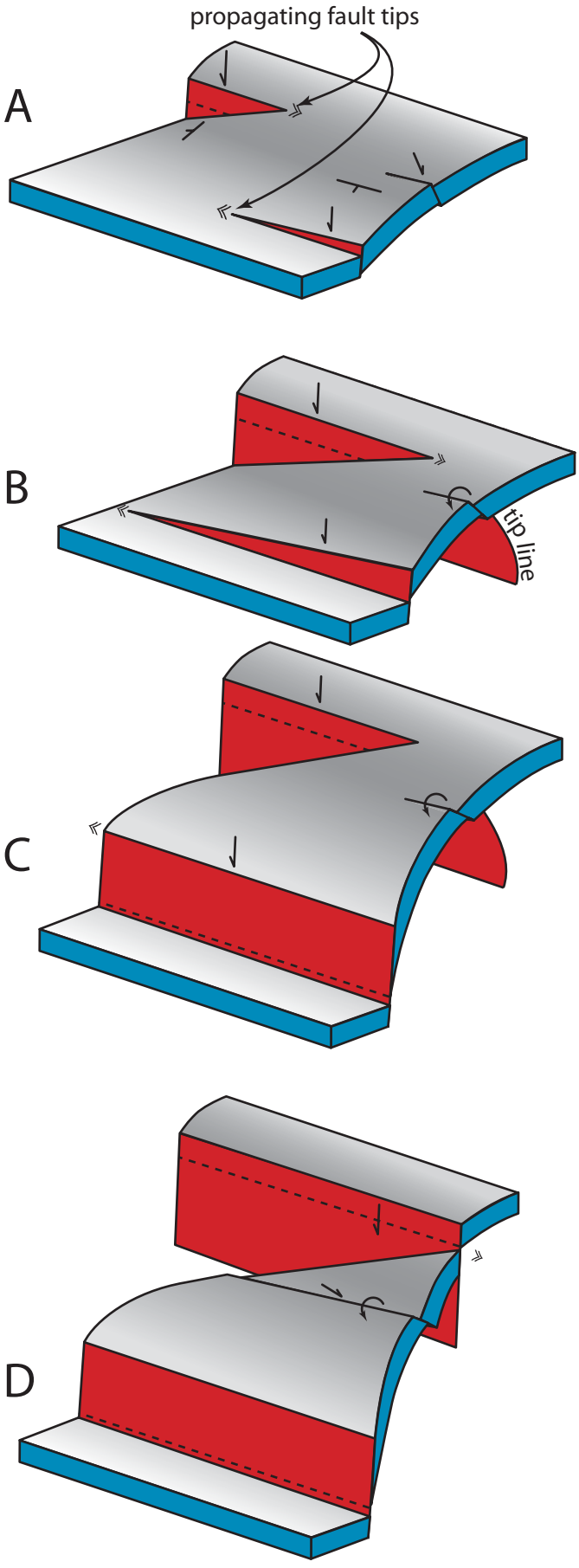

Figure 5-4. Development of complex fault zone architecture in the Upper Glen Rose Formation.

(A) Lateral propagation of two normal faults (propagation direction indicated by chevrons) establishes a relay ramp between the terminal sections of the faults. Bending in the relay ramp causes development of small extensional faults.

(B) Continued propagation of the bounding faults causes enlargement and increased bending of relay ramp. Early-formed normal faults in ramp become rotated.

(C) Continued propagation of one of the bounding faults, propagation of other fault is arrested. Ramp steepens, and small faults within the ramp rotate.

(D) Temporarily-arrested fault propagates further. Relay ramp has rotated to become a synthetic dip panel and faults within the synthetic dip panel may be reactivated to accommodate down-dip extension.

6 FAULT BLOCK DEFORMATION

The magnitude of deformation and the orientations of small faults and fractures within fault blocks are major contributors to permeability anisotropy and connectivity within fault blocks (Sims et al., 2005). The evolution of extensional fault systems is characterized by nucleation and growth of numerous faults, which then become linked into a network of faults (Walsh and Watterson, 1988; Trudgill and Cartwright, 1994; Childs et al., 1995; Dawers and Anders, 1995; Cartwright and Mansfield, 1998; Ferrill et al., 1999a). During extensional fault system development, faults typically have displacement gradients along their lengths, which lead to deformation within adjacent fault blocks (Ferrill and Morris, 2001). Displacement variation along faults is common, and displacement gradients are typically steeper near fault terminations (tips) than on the fault as a whole (Dawers et al., 1993; Trudgill and Cartwright, 1994; Dawers and Anders, 1995). The presence of a displacement gradient requires that, in most cases, either one or both of the hanging wall and footwall cutoff lines must differ in length from their original, prefaulted lengths. Factors that influence the magnitude and partitioning of strain between footwall and hanging wall cutoffs include (i) dip of fault, (ii) displacement gradient on fault, (iii) degree of footwall uplift versus hanging wall subsidence, and (iv) orientation of fault slip vector.

Ferrill and Morris (2001) developed a methodology that estimates fault block strain based on present-day geometry of the horizon/fault intersection lines (cutoff lines), original cutoff line orientations, and fault slip directions. We used this approach to calculate cutoff line elongations for cutoff lines from the three-dimensional model. Cutoff lines used in the analysis are from the top of the Edwards (Georgetown Formation; Figure 6-1). We used 3DStress™ to calculate slip directions for all fault surfaces in fault gaps, using the 3-dimensional orientations for each fault segment, and the stress tensor determined based on fault analyses conducted in this project (see Section 4.3 for details) where σ_1' = vertical = 15 MPa, σ_2' = azimuth 060 = 9.5 MPa; σ_3' = azimuth 150 = 4 MPa). Resulting cutoff line elongations tend to be very small; only in rare cases do elongations exceed 2 percent (positive or negative). These small cutoff elongations reflect the low displacement gradients on faults as characterized in the Helotes geologic framework model.

Observations at the scale of the three-dimensional geologic framework model of very gentle dips in competent units (e.g., massive limestones) are consistent with relatively rapid lateral and vertical propagation, until intersection with other faults occurs (laterally) or intersection with a weaker mechanical layer occurs. This lack of steep lateral displacement suggests rapid fault propagation with respect to the rate of displacement accumulation on the faults (Ferrill and Morris, 2001). Relatively rapid lateral propagation with respect to displacement accumulation resulted in comparatively small displacement gradients on faults, little cutoff elongation, and relatively minor influence on fault block deformation. Map scale faults at high angles to regional fault trends are mapped and may accommodate cutoff extension.

Although cutoff elongation strains are generally low, there are areas of higher strains. In general, these are along faults or sections of faults that are not aligned with the regional trend (Figures 4-6 and 6-1). This is especially true of faults south of the Haby Crossing fault that have east to west or east-southeast to west-northwest trends. These faults probably accommodate relay ramp extensions associated with the large-scale San Antonio relay ramp (see section 4.3, above), and their cutoff elongation strain values are not valid for the stress system used in this analysis. However, the presence of these faults illustrates the importance of cutoff elongation and relay ramp strains at a larger scale - that of the San Antonio, and similar, relay ramps (Collins, 1993). Faults with this orientation, or with northwest to southeast strikes are common throughout the Balcones Fault zone (e.g., Barker et al., 1994; Ferrill et al., 2003, 2004).

Adjacent to a segment of the Hidden Valley fault are small-displacement faults (8 to 15 cm, 3 to 6 inches) with northwest to southeast strikes that accommodate cutoff elongation generated by displacement gradients on the Hidden Valley fault system (Figure 6-2). In addition, the fault interpreted to lie below the monocline illustrated in Figure 5-1b has this orientation but is beneath the resolution of the 3-dimensional framework model of this study. This fault trend may also be reflected in the southeastward dip of the potentiometric surface in this area (see figure 7 in LBG-Guyton Associates, 1995).

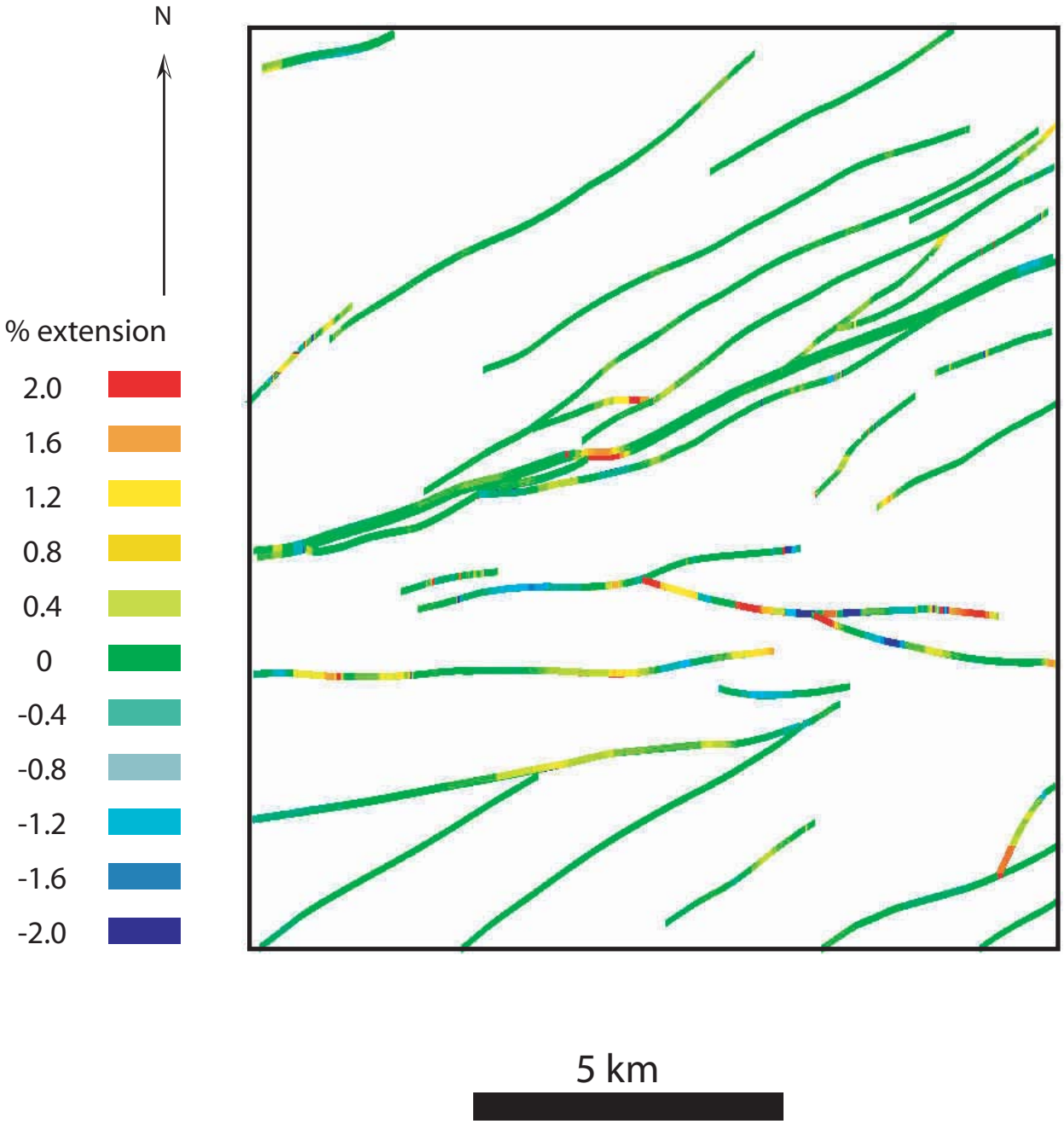

Figure 6-1. Fault cutoff elongation map for the top of the Edwards Aquifer (Georgetown-Person Formations) based on fault gaps in the Helotes geologic framework model.

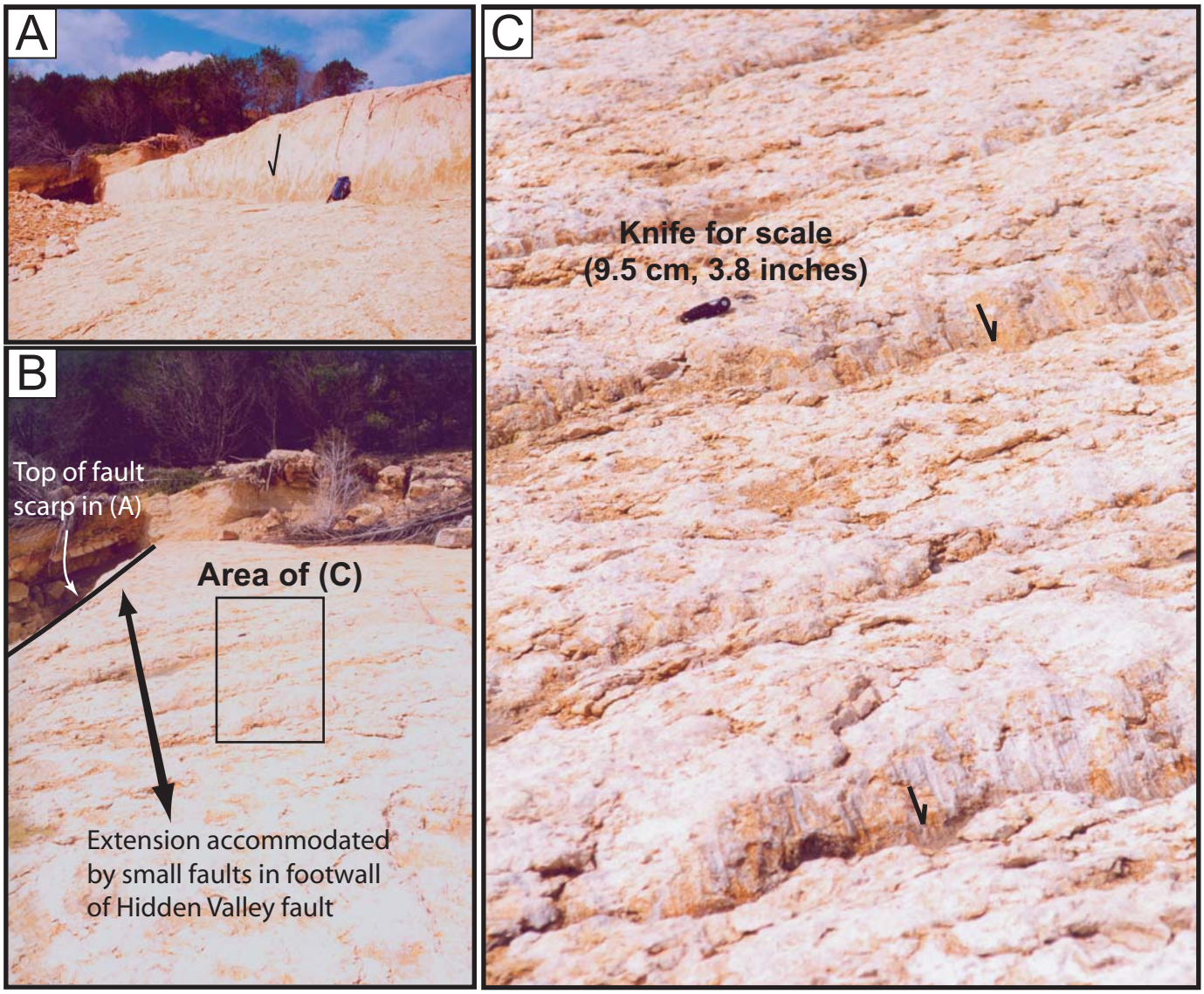

Figure 6-2. Cutoff elongation accommodated by small-displacement faults adjacent to the Hidden Valley fault exposed in the Canyon Lake spillway gorge. (A) View of the Hidden Valley fault scarp looking west-northwest. Fractures visible above the backpack are the branch lines of faults illustrated in (B) and (C). (B) View of the footwall of the fault scarp illustrated in (A). Small-displacement fault scarps traverse the view from left to right. (C) Detail of area indicated in (B).

7 STRUCTURAL ANALYSIS OF POTENTIAL COMMUNICATION BETWEEN EDWARDS AND TRINITY AQUIFERS

The contribution of water to the Edwards from the Trinity Aquifer has been the subject of a range of investigations that considered the geology, geochemistry, and hydrologic modeling of the interface between the two aquifer systems. These investigations have resulted in a wide range of estimates of the contribution of water from the Trinity to the Edwards Aquifer (see discussion by Mace et al., 2000, in section on "Discharge" for a summary of the different interpretations). LBG-Guyton Associates (1995) specifically investigated the aquifer interface along the Haby Crossing fault where fault throw has fully juxtaposed the Edwards and Glen Rose limestones. As discussed in Section 4, although fault throws of this magnitude are not present in the Camp Bullis and Castle Hills area, lateral increase in displacement on the Haby Crossing fault results in more than 100 m (328 ft) of throw and juxtaposition of the Edwards Aquifer against the Glen Rose Formation across the Haby Crossing fault (see section 4.2, above, and Figure 4-5) along its entire length in the Helotes area.

The Haby Crossing fault represents a large exposure of the Edwards Aquifer to water from the Glen Rose Formation (Figure 4-5). Although the geochemical modeling presented by LBG-Guyton Associates (1995) estimates that less than 5 percent of the Edwards recharge in the Haby Crossing fault area is attributable to water from the Glen Rose, we believe that the Glen Rose contribution could be much greater than this. There are three lines of reasoning that lead to this conclusion: (i) the area of Glen Rose juxtaposed with Edwards throughout the Helotes area along the Haby Crossing fault; (ii) the geometry of the potentiometric surface in the Helotes area and adjacent to the Haby Crossing fault (as mapped by LBG-Guyton Associates (1995)); (iii) the possibility that the Glen Rose Formation does not have a simple geochemical signature that can be used in a mixing model.

Between 68 and 100 percent of the total Edwards thickness is juxtaposed with the Glen Rose Formation across the entire Helotes area. Although faults within the Edwards and Glen Rose sections can seal, they are most commonly complex, with both sealed and permeable portions likely to occur within the same fault zone. Field observations indicate that large-displacement faults are not barriers, but instead localize complex flow pathways that provide opportunities for fluid to flow within the fault zone and to cross the fault. Even in the Upper Glen Rose Formation, where clay smear into faults is common (Ferrill et al., 2003), large-displacement faults (10's to 100's m) are most commonly conduits for flow (e.g., Figure 7-1) and can localize karst dissolution and development of high-transmissivity zones.

The potentiometric surface within the Glen Rose Formation north of the Haby Crossing fault dips steeply toward the fault. Immediately south of the fault, the potentiometric surface in the Edwards has a gentle, south-eastward slope (e.g., LBG-Guyton Associates, 1995). This potentiometric surface geometry indicates flow within the Glen Rose Formation toward the Haby Crossing fault. Across (down-gradient from) the Haby Crossing fault the southeastward potentiometric gradient suggests flow away from the fault within the Edwards in an area where the Glen Rose Formation is juxtaposed by faulting against the Edwards. Our assessment of the potentiometric surface presented by LBG-Guyton Associates (1995) leads us to the conclusion that the principal source of water for the Edwards in this area is the Haby Crossing fault. Potential sources of water in the fault include surface recharge directly into the fault, upward flow along the fault, lateral flow along the fault, and across-fault flow from the Glen Rose Formation immediately to the north.

Geochemical modeling of the potential contribution of Glen Rose Formation water to the Edwards Aquifer in the area of the Haby Crossing fault (LBG-Guyton Associates, 1995) assumes that the Glen

Rose Formation has a specific geochemical signature. However, the Glen Rose Formation is composed of many lithologic layers (limestone aquifers and clay rich aquitards), and it is likely that the chemistry of Lower Glen Rose water is significantly different from that of Upper Glen Rose water. There are likely to be geochemical differences between aquifer water with long residence times (higher salinity) and water with shorter residence times in more transmissive zones (lower salinity) that form fast flow paths (Hovorka et al., 2004). Wells used in the modeling analysis (LBG-Guyton Associates, 1995) are variable in depth and exposed to different stratigraphic sections and the contributions of these different units were not determined and analyzed. There is also a general increase in total dissolved solids and content of the measured solutes to the west reported in the pre-modeling well analysis. In addition, there is potential for karst features within the Upper Glen Rose Formation to contribute water that is essentially surface runoff diverted into cave systems along drainage features such as Los Reyes Creek and Chimenea Creek (Figure 3-1). The residence time of such water in the subsurface is not known, but if on the order of days to weeks, it could provide relatively fresh water to the Edwards through the Glen Rose.

The structural analyses presented in this report provide the framework for more focused investigations, including determining groundwater levels, single well and multiwell pumping (drawdown) tests, tracer studies, and geochemical investigations to further investigate potential groundwater communication between the Edwards and Trinity Aquifers in the Helotes Quadrangle area.

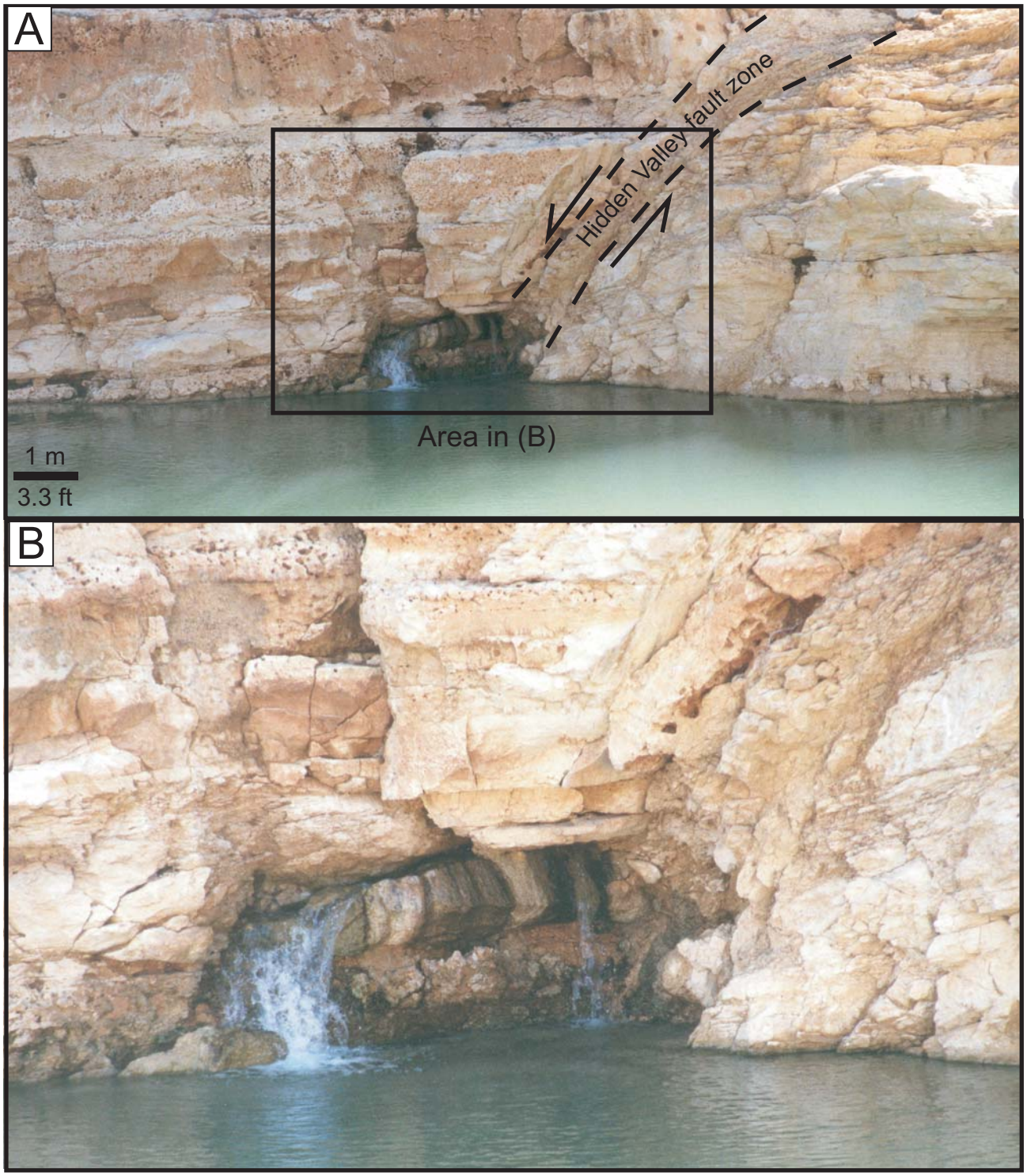

Figure 7-1. Photograph of Hidden Valley fault zone exposed in the Canyon Lake spillway gorge. (A) Fault zone discharging water. (B) Detail of area indicated in (A).

8 SUMMARY

The purpose of the project reported here was to characterize the structural architecture of the Edwards and Trinity Aquifers for the area of the Helotes 7 ½ minute quadrangle. Included in this analysis were tasks to generate a three-dimensional computer model of the Edwards and Trinity Aquifer and perform field investigations to characterize the mechanisms and products of localized fault-related deformation in the Edwards Aquifer and Trinity Aquifer near the study area. An important objective was to analyze the potential for communication between the Edwards Aquifer and the Trinity Aquifers, taking into account fault-related deformation and juxtaposition of the aquifers across key faults. We investigated the geologic structure of the Edwards and Trinity Aquifers to assess the large scale aquifer architecture, analyze fault offset and stratigraphic juxtaposition relationships, evaluate fault zone deformation and dissolution and fault system architecture, and investigate fault block deformation including small scale (intra block) normal faults. The goal was to assess the structural controls on the aquifers at a broad range of scales that may influence water movement.

Comparing field observations and data from this project with results of previous projects has led to a new understanding of fault-related deformation for the limestones of the Glen Rose Formation that contrasts with the deformation style in the Edwards Group Limestone. Faults with displacements of 5 m (16 ft) to tens of meters in the Glen Rose Formation commonly have damage zones with widths on the order of meters, within which small faults and rotated fault blocks are common. Faults with displacements of 5 m (16 ft) to tens of meters in the Edwards Group limestones typically have numerous associated small faults, but block rotation and bed tilting are not common. This characteristic difference in structural style between the Edwards Group limestones and the Glen Rose Formation appears to be related to lithologic differences and the resulting differences in mechanical behavior of the two stratigraphic sections. The Glen Rose Formation is more heterolithic, containing competent massive limestone beds interbedded with incompetent argillaceous limestone and shale beds. Incompetent beds tend to arrest fault propagation during fault growth. Consequently, with increasing fault displacement, fault tips propagate episodically. Continued displacement on a fault with an arrested fault tipline will produce fault tipline folding and associated local deformation such as intense small scale faulting. Continued fault tip propagation breaks through the zone containing the tipline fold and locally intense faulting. During continued displacement, distributed deformation in the damage zone may continue to occur, rotating bedding and small faults and shear relatively incompetent beds. Resulting fault damage zones can be quite complex and variable along a fault, related to the structural position (including displacement magnitude) and the associated mechanical stratigraphy. Permeability in fault zones and fault blocks is likely to be strongly influenced by the different deformation styles in mechanical layers and the deformation progression with increasing fault displacement.

Extensional deformation in the Helotes study area has produced a network of faults likely to influence intra-aquifer permeability due to fault zone processes producing permeability anisotropy with maximum transmissivity parallel to fault strike. This effect is accentuated by the fact that displacement on these faults has thinned the aquifer along each fault, further restricting aquifer connectivity perpendicular to fault strike. Many of these faults do not have major displacement. However, the Haby Crossing fault juxtaposes almost the entire Edwards Aquifer with the Glen Rose Formation across the width of the Helotes quadrangle. The maximum vertical displacement mapped on the Haby Crossing fault in the Helotes study area is approximately 178 m (584 ft), and displacement consistently exceeds 100 m (328 ft). Displacement on the Haby Crossing fault in the Helotes area and to the west, juxtaposes 68–100 percent of the Edwards Aquifer stratal thickness against Glen Rose strata, providing the opportunity for inter-aquifer communication. Reassessment of a published potentiometric surface map leads to the

conclusion that the major contributor to water in the Edwards Aquifer in the Helotes area is the Haby Crossing fault. Potential sources of water along the Haby Crossing fault include surface recharge directly into the fault, upward flow along the fault, lateral flow along the fault, and across-fault flow from the Glen Rose directly to the north.

9 REFERENCES

Allan, U.S., 1989, Model for hydrocarbon migration and entrapment within faulted structures: Bulletin of the American Association of Petroleum Geologists, v. 73, p. 803–811.

Antonellini, M., and Aydin, A., 1994, Effect of faulting on fluid flow in porous sandstones: Petrophysical properties: Bulletin of the American Association of Petroleum Geologists, v. 78, p. 355–377.

Arnow, T., 1963, Ground-water geology of Bexar County, Texas: U.S. Geological Survey Water-Supply Paper 1588, 36 p., 13 plates.

Ashworth, J. B., 1983, Ground-water availability of the lower Cretaceous formations in the Hill Country of South-Central Texas, Texas Department of Water Resources, Report 273.

Barker, R.A., Bush, P.W., and Baker, E.T., Jr., 1994, Geologic history and hydrogeologic setting of the Edwards-Trinity Aquifer system, west-central Texas: U.S. Geological Survey, Water-Resources Investigations Report 94–4039, 51 p.

Caine, J. S., Evans, J.P., and Forster, C.B. 1996, Fault zone architecture and permeability structure: Geology, v. 24, p. 1,025–1,028.

Cartwright, J.A., and Mansfield, C.S., 1998, Lateral displacement variation and lateral tip geometry of normal faults in the Canyonlands National Park, Utah: Journal of Structural Geology, v. 20, p. 3–19.

Chalk Butte Inc., 1994, U.S. Digital Topography for GIS. Boulder, Wyoming: Chalk Butte Inc.

Childs, C., Watterson, J., and Walsh, J.J., 1995, Fault overlap zones within developing normal fault systems: Journal of the Geological Society, London, v. 152, p. 535–549.

Childs, C., Nicol, A., Walsh, J.J., and Watterson, J., 1996, Growth of vertically segmented normal faults: Journal of Structural Geology, v. 18, p. 1389–1397.

Clark, A.K., 2000, Vulnerability of ground water to contamination, Edwards Aquifer recharge zone, Bexar County, Texas, 1998: U.S. Geological Survey Water-Resources Investigations Report 00-4149, 9 p., 1 sheet.

Collins, E.W., 1993, Fracture zones between overlapping *en echelon* fault strands: outcrop analogs within the Balcones fault zone, central Texas: Gulf Coast Association of Geological Societies Transactions, v. 43, p. 77–85.

Collins, E.W., 2000, Geologic map of the New Braunfels, Texas, 30×60 minute quadrangle: geologic framework of an urban-growth corridor along the Edwards Aquifer, south-central Texas: The University of Texas at Austin Bureau of Economic Geology Miscellaneous Map No. 39, 28 p., scale 1:100,000, 1 sheet.

Collins, E.W., and Hovorka, S.D., 1997, Structure map of the San Antonio segment of the Edwards Aquifer and Balcones fault zone, south-central Texas: Structural framework of a major limestone aquifer: Kinney, Uvalde, Medina, Bexar, Comal, and Hays Counties: The University of Texas at Austin, Bureau of Economic Geology, Miscellaneous Map No. 38, scale 1:250,000, 2 sheets.

Dawers, N.H., Anders, M.H., and Scholz, C.H., 1993, Growth of normal faults: Displacement-length scaling: Geology, v. 21, p. 1107–1110.

Dawers, N.H., and Anders, M.H., 1995, Displacement-length scaling and fault linkage: Journal of Structural Geology, v. 17, p. 607–614.

Deike, R.G., 1990, Dolomite dissolution rates and possible Holocene dedolomitization of water-bearing units in the Edwards Aquifer, south-central Texas: Journal of Hydrology, v. 112, p. 335–373.

Dynamic Graphics, Inc., 2001, EarthVision User's Guide, Version 6.0. Alameda, CA: Dynamic Graphics, Inc.

Ferrill, D.A., and Morris, A.P., 2001, Displacement gradient and deformation in normal fault systems: Journal of Structural Geology, v. 23, p. 619-638.

Ferrill, D.A., and Morris, A.P., 2003. Dilational normal faults: Journal of Structural Geology, v. 25, p. 183–196.

Ferrill, D.A., Morris, A.P., Stamatakos, J.A., and Sims, D.W., 2000, Crossing conjugate normal faults: Bulletin of the American Association of Petroleum Geologists, v. 84, p. 1543–1559.

Ferrill, D.A., Sims, D.W., Morris, A.P., Waiting, D.J., and Franklin, N., 2003, *Structural Controls on the Edwards Aquifer/Trinity Aquifer Interface in the Camp Bullis Quadrangle, Texas.* Final Report to Edwards Aquifer Authority, San Antonio, Texas.

Ferrill, D.A., Sims, D.W., Waiting, D.J., Morris, A.P., Franklin, N., Schultz, A.L., 2004. Structural Framework of the Edwards Aquifer recharge zone in south-central Texas. Geological Society of America Bulletin, v. 116, p. 407-418.

Ferrill, D.A., Morris, A.P., Sims, D.W., Waiting, D.J., Hasegawa, S., 2005. Development of synthetic layer dip adjacent to normal faults. In Sorkhabi, R. (Ed.), Traps and Seals. AAPG Memoir, American Association of Petroleum Geologists, Tulsa, OK, USA, (in press).

Ferrill, D.A., Stamatakos, J.A., and Sims, D.W., 1999a, Normal fault corrugation: Implications for growth and seismicity of active normal faults: Journal of Structural Geology, v. 21, p. 1027–1038.

Ferrill, D.A., Winterle, J., Wittmeyer, G., Sims, D.W., Colton, S., Armstrong, A., and Morris, A.P., 1999b. Stressed rock strains groundwater at Yucca Mountain, Nevada: GSA Today, v. 9, no. 5, p. 1–8.

Finkbeiner, T., Barton, C.A., and Zoback, M.D., 1997, Relationships among *in-situ* stress, fractures and faults, and fluid flow: Monterey Formation, Santa Maria Basin, California: Bulletin of the American Association of Petroleum Geologists, v. 81, p. 1975–1999.

Foley, L.L., 1926, Mechanics of the Balcones and Mexia faulting: Bulletin of the American Association of Petroleum Geologists, v. 10, no. 12, p. 1261–1269.

George, W. O., 1952, Geology and Ground-Water Resources of Comal County, Texas: U. S. Geological Survey Water-Supply Paper 1138.

Grimshaw, T.W., Woodruff, C.M., Jr., 1986, Structural style in an *en echelon* fault system, Balcones fault zone, central Texas: geomorphologic and hydrologic implications: *in* Abbott, P.L., and Woodruff, C.M., Jr., eds. 1986. The Balcones Escarpment, Central Texas: Geological Society of America, p. 71–76.

Groschen, G.E., 1996, Hydrogeologic factors that affect the flowpath of water in selected zones of the Edwards Aquifer, San Antonio region, Texas: U.S. Geological Survey Water-Resources Investigations 96-4046, 73 p.

Hanson, J.A., and Small, T.A., 1995, Geologic framework and hydrogeologic characteristics of the Edwards Aquifer outcrop, Hays County, Texas: U.S. Geologic Survey Water-Resources Investigations Report 95-4265, 10 p.

Hayes, M.E., 2000, Major Aquifers of Texas (map), Texas Water Development Board (TWDB), Austin, Texas: website: http://www.twdb.state.tx.us/mapping/maps/pdf/aqu_maj_24x24.pdf

Hovorka, S.D., Mace, R.E., and Collins, E.W., 1998, Permeability structure of the Edwards Aquifer, South Texas—Implications for aquifer management: The University of Texas at Austin, Bureau of Economic Geology Report of Investigations, v. 250, 55 p.

Hovorka, S.D., Phu, T., Nicot, J.P., and Lindley, A., 2004, Refining the conceptual model for flow in the Edwards Aquifer—Characterizing the role of fractures and conduits in the Balcones fault zone segment. Final contract report to the Edwards Aquifer Authority: The University of Texas at Austin, Bureau of Economic Geology.

Huggins, P., Watterson, J., Walsh, J.J., and Childs, C., 1995, Relay zone geometry and displacement transfer between normal faults recorded in coal-mine plans: Journal of Structural Geology, v. 17, p. 1741–1755.

Johnson, S., Esquilin, R., Mahula, D.M., Thompson, E.L., Mireles, J., Gloyd, R., Sterzenback, J., Hoyt, J.R., and Schindel, G., 2002, Hydrogeologic Data Report for 2001. Edwards Aquifer Authority, p. 1-3.

Kastning, E.H., 1981, Tectonism, fractures, and speleogenesis in the Edwards Plateau, Central Texas: *in* Beck, B.F., ed., Eighth International Congress of Speleology, Bowling Green, Ky., July 18–24, 1981, Proceedings, Hunstville, Alabama, National Speleological Society Bulletin, v. 2, p. 692–695.

Knipe, R.J., 1997, Juxtaposition and seal diagrams to help analyze fault seals in hydrocarbon reservoirs: Bulletin of the American Association of Petroleum Geologists, v. 81, p. 187–195.

Kuniansky, E.L., and Holligan K.Q. 1994. Simulations of flow in the Edwards-Trinity Aquifer system and contiguous hydraulically connected units, west-central Texas. U.S. Geological Survey Water-Resources Investigations Report 93-4039, 40 p.

LBG-Guyton Associates, 1995, Edwards/Glen Rose Hydrologic Communication, San Antonio Region, Texas.: Final report for the Edwards Underground Water District, 38 p. with 7 Tables, 13 Figures, and 4 appendices.

Larsen, P.-H., 1988, Relay structures in a lower Permian basement-involved extension system, East Greenland: Journal of Structural Geology, v. 10, p. 3–8.

Loucks, R.G., 1999, Paleocave carbonate reservoirs: origins, burial-depth modifications, spatial complexity, and Reservoir implications: American Association of Petroleum Geologists Bulletin, v. 83, no. 11, p. 1795–1834.

Mace, R.E., Chowdhury, A.H., Anaya, R., and Way, S.-C. 2000. Groundwater availability of the Trinity Aquifer, Hill Country Area, Texas: Numerical simulations through 2050. Texas Water Development Board, Austin, Texas, 169 p.

Maclay, R.W., 1989, Edwards Aquifer in San Antonio: Its hydrogeology and management: South Texas Geological Society Bulletin, v. 30, no. 4, p. 11–28.

Maclay, R.W., 1995, Geology and Hydrology of the Edwards Aquifer in the San Antonio Area, Texas: U.S. Geological Survey Water-Resources Investigations Report 95-4186, 64 p., 12 plates.

Maclay, R.W., and Rettman, P.L., 1972, Hydrologic Investigations of the Edwards and Associated Limestones in the San Antonio Area, Texas, Progress Report, 1970–1971: U.S. Geological Survey Open-File Report 72-244, 24 p.

Maclay, R.W., and Small, T.A., 1976, Progress report on geology of the Edwards Aquifer, San Antonio area, Texas, and preliminary interpretation of borehole geophysical and laboratory data on carbonate rocks: U.S. Geological Survey, Open-File Report 76-627, 65 p.

Maclay, R.W., and Small, T.A., 1983, Hydrostratigraphic subdivisions and fault barriers of the Edwards Aquifer, south-central Texas, U.S.A.: Journal of Hydrology, v. 61, p. 127–146.

Maclay, R.W., and Small, T.A., 1984, Carbonate geology and hydrology of the Edwards Aquifer in the San Antonio area, Texas: U.S. Geological Survey Open-File Report OFR 83-537, 72 p., 14 sheets.

Mayer, J.R., and Sharp, J.M., Jr., 1998, Fracture control of regional ground-water flow in a carbonate aquifer in a semi-arid region: GSA Bulletin, v. 110, no. 2, p. 269–283.

Morris, A.P., Ferrill, D.A., and Henderson, D.B., 1996, Slip-tendency analysis and fault reactivation: Geology, v. 24, no. 3, p. 275–278.

Morris, A.P., Ferrill, D.A. 1999, Constant-thickness deformation above curved normal faults: Journal of Structural Geology, v. 21, p. 67–83.

Murray, G. E., 1956, Relationships of Paleozoic structures to large anomalies of coastal element of eastern North America: Gulf Coast Association of Geological Societies Transactions, v. 6, p. 13–24.

Murray, G. E., 1961, Geology of the Atlantic and Gulf Coastal Province of North America: New York, Harper and Brothers, 692 pp.
Needham, J., 2001a, Chemical weapon dump is posing aquifer threat, Camp Bullis site focus of concern: San Antonio Express News, July 1, 2001, p. 1A and 9A.
Needham, J., 2001b, Wells near Army post are tainted, bottled water given out in Camp Stanley area: San Antonio Express News, August 6, 2001, p. 1A and 12A.
Palmer, A.N., 1991, Origin and morphology of limestone caves: Geological Society of America Bulletin, v. 103, p. 1-21.
Peacock, D.C.P., and Sanderson, D.J., 1994, Geometry and development of relay ramps in normal fault systems: Bulletin of the American Association of Petroleum Geologists, v. 78, p. 147–165.
Pearson, S., and Murphy, B. 2004. A case study of traditional and alternative monitoring techniques for solvent contamination within fractured bedrock. Proceedings of 2004 U.S. EPA/NGWA Fractured Rock Conference: State of the Science and Measuring Success in Remediation, national Ground Water Association, Westerville, OH, p. 239–252.
Reeves, R.D., 1972, Maps showing outcrops of the Edwards and associated limestones in the principal recharge area of the Edwards Aquifer in Bexar County, Texas: U.S. Geological Survey Open-File Report OF 72-0310, 6 sheets.
Rose, P.R., 1972, Edwards Group, surface and subsurface, central Texas: University of Texas, Bureau of Economic Geology Report of Investigations 74, 198 p.
Sharp, J.M., Jr., and Banner, J.L., 1997, The Edwards Aquifer: A resource in conflict: GSA Today, v. 7, p. 1–9.
Shaw, S.L., 1978, Structural Geology of the Edwards Aquifer in the Castle Hills Quadrangle, Northwestern San Antonio, Texas: The Texas Journal of Science, v. XXX, no. 2, p. 125–131.
Sims, D.W., Morris, A.P., Ferrill, D.A., and Sorkhabi, R. 2005. Extensional fault system evolution and Reservoir connectivity. In Sorkhabi, R. (Ed.), Traps and Seals. AAPG Memoir, American Association of Petroleum Geologists, Tulsa, OK, USA, (in press).
Small, T.A., 1984, Identification and Tabulation of Geologic Contacts in the Edwards Aquifer, San Antonio Area, Texas: U.S. Geological Survey Open-File Report 84-075, 54 p.
Small, T.A., 1985, Identification and Tabulation of Geologic Contacts in the Edwards Aquifer, San Antonio Area, Texas: U.S. Texas Department of Water Resources, LP-199, Austin, Texas.
Small, T.A., and Clark, A.K., 2000, Geologic Framework and Hydrogeologic Characteristics of the Edwards Aquifer Outcrop, Medina, County, Texas: U.S. Geological Survey Water-Resources Investigations Report 00-4195, 10 p., 1 plate.
Small, T.A., and Hanson, J.A., 1994, Geologic framework and hydrogeologic characteristics of the Edwards Aquifer outcrop, Comal County, Texas: U.S. Survey Water-Resources Investigations Report 94-4117, 1:75,000 scale, 10p., 1 plate.
Southwest Research Institute, 2003. 3DStress™ Version 3.0 User's Guide, Southwest Research Institute: San Antonio, Texas.
Stein, W.G., and Ozuna, G.B., 1996, Geological framework and hydrogeologic characteristics of the Edwards Aquifer recharge zone, Bexar County, Texas. U.S. Geological Survey Water-Resources Investigations Report 95-4030, 1:75,000 scale, 8 p., 1 plate.
Texas Natural Resources Information System (TNRIS), 1997, Digital coverage of Major Texas Aquifers source Texas Water Development Board, Austin, Texas: TNRIS, website: ftp://ftp.tnris.state.tx.us/Water_Resources/Ground_Water/Maj_Aqu_DD/
Trudgill, B., and Cartwright, J., 1994, Relay-ramp forms and normal-fault linkages, Canyonlands National Park, Utah: Geological Society of America Bulletin, v. 106, p. 1143–1157.

Waiting, D.J., Ferrill, D.A., Sims, D.W., 2003, Development of a high-resolution geological framework model for the Edwards Aquifer Recharge Zone: Data, assumptions, procedures, and workflow, South Texas Geological Society Bulletin, v. XLIII, no. 7, p. 13-24.

Walsh, J.J. and Watterson, J. 1988, Dips of normal faults in British coal measures and other sedimentary sequences: Journal of the Geological Society London, v. 145, p. 859-873.

Waterreus, P.A., 1992. Hydrogeology of the Camp Bullis Area, northern Bexar County, Texas [Masters Thesis]: The University of Texas at San Antonio, 186 p.

Weeks, A. W., 1945, Balcones, Luling, and Mexica fault zones in Texas: Bulletin of the American Association of Petroleum Geologists, v. 29, p. 1733–1737.

Wermund, E.G., and Cepeda, J.C., 1977, Regional relation of fracture zones to the Edwards Limestone Aquifer, Texas. in Tolson, J.S., and Doyle, F.L. Proceedings of the Twelfth International Congress Karst Hydrogeology. UAH Press, University of Alabama in Huntsville, Huntsville Alabama, USA, p. 239–253.

Wermund, E.G., Joseph, C.C., and Luttrell, P.E., 1978, Regional distribution of fractures in the southern Edwards plateau and their relationship to tectonics and caves: The University of Texas at Austin Bureau of Economic Geology Geologic Circular 78-2, 14 p.

Withjack, M.O., Olson, J., and Peterson, E., 1990, Experimental models of extensional forced folds: Bulletin of the American Association of Petroleum Geologists, v. 74, p. 1038–1054.

Yielding, G., Freeman, B., Needham, D.T., 1997, Quantitative fault seal prediction: Bulletin of the American Association of Petroleum Geologists, v. 81, p. 897–917.

Young, K., 1972, Mesozoic history, Llano region, *in* V.E., Barnes, W.C. Bell, S.E. Clabaugh, P.E. Cloud, Jr., R.V. McGehee, P.U. Rodda, and K. Young, eds., Geology of the Llano Region and Austin Area, Field Excursion: The University of Texas at Austin Bureau of Economic Geology Guidebook 13, 154 p.

Zahm, C.D., Marrett, R., and Sharp, J.M., Jr., 1998, Prediction of regional groundwater flow and permeability using fractured outcrop exposures, Edwards Aquifer, Central Texas: in Gambling with Ground Water – Physical, Chemical, and Biological Aspects of Aquifer-Stream Relations (eds., Brahana, J.V., Eckstein, Y., Ongley, L.K., Schneider, R., and Moore, J.E.), Proc., Joint Meeting. American Institute of Hydrology and XXVIII Congress I.A.H., Las Vegas, p. 697-705.

10 GLOSSARY

cataclasite - rock composed of broken rock fragments, resulting from fault slip
cataclastic - of or belonging to a cataclasite
cut-off line - line of intersection between a bed or horizon and a fault surface
décollement - detachment; surface (often near horizontal or parallel to bedding) that permits easy sliding (as of a fault), such as shale or salt
dilation - act of opening to form a void, as of a fracture
displacement gradient - rate at which displacement across a fault varies with position on the fault
en echelon - an array of parallel elements arranged in a zone that is oblique to each element
fault tip - point (in two dimensions) or line (in three-dimensions) that marks the end of a fault; bounding point or line of a fault beyond which there is no displacement
fault throw - vertical component of fault displacement
fault heave - horizontal component of fault displacement
footwall - displaced fault block that lies below the fault plane
hanging wall - displaced fault block that lies above the fault plane
hydrostatic stress - stress tensor in which all three principal stresses are equal; equivalent to pressure; stress acts equally in all directions as in a fluid
isochore - a line of equal value, e.g., contour, isobar etc.;
reference-isochore - the isochore from which others are measured
isopach map - map of lines of equal thickness for a given geological interval, layer, or formation

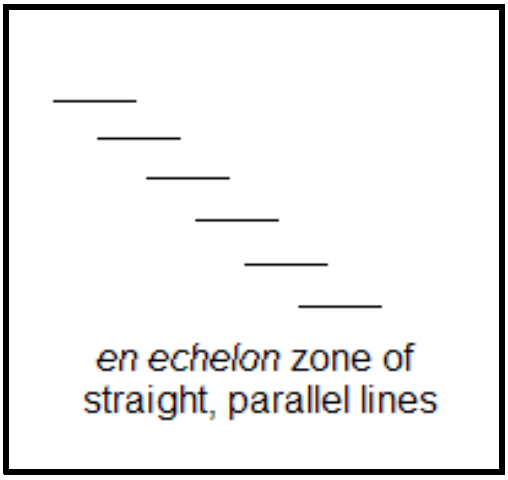

listric fault - concave upward fault surface (from Greek for shovel); also **anti-listric** - convex upward fault surface
lithostatic stress - the hydrostatic component of a stress tensor at some depth within the earth that results from the weight of overlying rock
mechanical stratigraphy - rock layers defined by their mechanical properties (strength, tendency to brittle or ductile behavior) rather than by their lithology or fossil content
monocline - rock layers dipping (tilted) in one direction; often separates areas where the rock layers are horizontal
normal fault - fault on which displacement has caused the hanging wall to move down relative to the footwall; usually associated with horizontal extension and a stress tensor that has vertical maximum principal stress
occlusion - something which obscures or covers up
pole - the pole to a surface is a line drawn perpendicular to that surface

relay ramp - region of intact rock that connects the hanging wall of a fault with its footwall

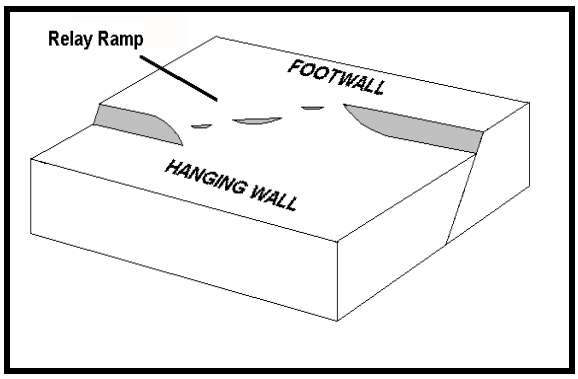

slickenlines - lines on a fault surface, either grooves or mineralized lineations, that indicate slip direction; may feel slick to the touch

slickolites - slickenlines that show evidence of mineral precipitation and dissolution

stress tensor - roughly synonymous with "stress system" and usually confined to homogeneous stress systems; most commonly defined by giving the magnitudes and orientations of the three mutually perpendicular principal stresses; specifying these implies a complete description of all possible stresses within the system

strike - the compass azimuth of a horizontal line drawn in a non-horizontal plane; the line of intersection between a plane and a horizontal surface

synthetic dip panels - rock layers adjacent to a fault or faults that have the same dip direction as the fault